

AD-A047 313

STATE UNIV OF NEW YORK AT BUFFALO AMHERST DEPT OF ELE--ETC F/6 9/3  
THE ALGORITHMIC GENERATION OF PSEUDO-OPTIMUM PULSE-BURST CODES.(U)  
SEP 77 J A CADZOW F30602-75-C-0122

UNCLASSIFIED

RADC-TR-77-312

NL

AD  
A047313



END  
DATE  
FILMED

1-78

DOC

AD A047313

RADC-TR-77-312  
Final Technical Report  
September 1977

12  
b.s.



THE ALGORITHMIC GENERATION OF PSEUDO-OPTIMUM  
PULSE-BURST CODES

State University of New York at Buffalo, Amherst

Dept of —

410477

Approved for public release; distribution unlimited.

AD No. —  
DDC FILE COPY

ROME AIR DEVELOPMENT CENTER  
Air Force Systems Command  
Griffis Air Force Base, New York 13441

DDC  
RECEIVED  
DEC 6 1977  
D

*Joseph L. Myerson*  
JOSEPH L. MYERSON  
Technical Director  
Surveillance Division

FOR THE COMMANDER:

*John P. Huss*  
JOHN P. HUSS  
Acting Chief, Plans Office

UNCLASSIFIED

SECURITY CLASSIFICATION OF THIS PAGE (When Data Entered)

19 REPORT DOCUMENTATION PAGE		READ INSTRUCTIONS BEFORE COMPLETING FORM
1 REPORT NUMBER 18 RADCTR-77-312	2 GOVT ACCESSION NO.	3 RECIPIENT'S CATALOG NUMBER 9
4 TITLE (and Subtitle) 6 THE ALGORITHMIC GENERATION OF PSEUDO-OPTIMUM PULSE-BURST CODES		5 TYPE OF REPORT & PERIOD COVERED Final Technical Report, 1 Jun 77 - 1 Aug 77
7 AUTHOR (last, first) 10 Dr. James A. Cadzow		6 PERFORMING ORG. REPORT NUMBER N/A
	15 F30602-75-C-0122	8 CONTRACT OR GRANT NUMBER(s)
9 PERFORMING ORGANIZATION NAME AND ADDRESS Department of Elec. Engineering State University of New York at Buffalo Amherst NY 14260		10. PROGRAM ELEMENT, PROJECT, TASK AREA & WORK UNIT NUMBERS 62702F 4506001
11. CONTROLLING OFFICE NAME AND ADDRESS Rome Air Development Center (OCTS) Griffiss AFB NY 13441	11	12. REPORT DATE Sep 77
14 MONITORING AGENCY NAME & ADDRESS (if different from Controlling Office) Same		13. NUMBER OF PAGES 60
		15. SECURITY CLASS. (of this report) UNCLASSIFIED
16 DISTRIBUTION STATEMENT (of this Report) Approved for public release; distribution unlimited.		15a. DECLASSIFICATION/DOWNGRADING SCHEDULE N/A
17 DISTRIBUTION STATEMENT (of the abstract entered here, if different from Report) Same		
18. SUPPLEMENTARY NOTES RADC Project Engineer: Paul VanEtten (OCTS)		
19 KEY WORDS (Continue on reverse side if necessary and identify by block number) Signal Processing Pulse Compression Pulse-Burst Waveforms		
20 ABSTRACT (Continue on reverse side if necessary and identify by block number) This report describes some initial results in the algorithmic generation of finite length pulse-burst signals whose autocorrelation functions are approximately impulse-like in nature. The codes will be restricted to be real with piecewise constant amplitude that can either be positive or negative (i.e., bi-phase). Such codes find various applications in radar signal processing and digital communication systems. A new pulse-burst code is presented and compared with the Barker and Hoffman codes.		

DD FORM 1473 EDITION OF 1 NOV 65 IS OBSOLETE

UNCLASSIFIED

SECURITY CLASSIFICATION OF THIS PAGE (When Data Entered)

410477

Jace



UNCLASSIFIED

SECURITY CLASSIFICATION OF THIS PAGE(When Data Entered)

UNCLASSIFIED

SECURITY CLASSIFICATION OF THIS PAGE(When Data Entered)

# TABLE OF CONTENTS

## Section

1.	INTRODUCTION . . . . .	1
1.1	PURPOSE . . . . .	1
1.2	BACKGROUND . . . . .	1
2.	RADAR SIGNAL DESCRIPTION . . . . .	2
2.1	BASIC SIGNAL MODEL . . . . .	2
2.2	TARGET RESOLUTION AND THE AMBIGUITY FUNCTION . . . . .	4
2.3	THE MATCHED FILTER . . . . .	7
2.4	AUTOCORRELATION FUNCTION . . . . .	9
3.	PULSE-BURST SIGNALS . . . . .	12
3.1	BASIC DEFINITIONS . . . . .	12
3.2	AUTOCORRELATION . . . . .	14
3.3	QUALITY MEASURES . . . . .	15
3.4	CONSTANT MAGNITUDE CODES . . . . .	17
3.5	HUFFMAN CODES . . . . .	21
4.	ALGORITHMIC GENERATION OF REAL PULSE-BURST CODES	
4.1	INTRODUCTION . . . . .	27
4.2	PSEUDO-OPTIMUM CODES . . . . .	27
4.3	NONRECURSIVE MODEL . . . . .	30
4.4	LINEARIZATION ALGORITHM . . . . .	31
4.5	INITIAL CODE SELECTION . . . . .	35
5.	NUMERICAL RESULTS	
5.1	PSEUDO-OPTIMUM CODE OF LENGTH 11 . . . . .	37
5.2	PSEUDO-OPTIMUM CODE OF LENGTH 128 . . . . .	42
6.	CONCLUSIONS AND RECOMMENDATIONS . . . . .	45
7.	REFERENCES . . . . .	46
8.	APPENDICES	
8.1	AMBIGUITY FUNCTION PLOT PROGRAM . . . . .	47
8.2	PSEUDO-OPTIMUM CODE ALGORITHM PROGRAM . . . . .	53

ACCESSION for	
NTIS	White Section <input checked="" type="checkbox"/>
DDC	Buff Section <input type="checkbox"/>
UNANNOUNCED	<input type="checkbox"/>
JUSTIFICATION.....	
BY.....	
DISTRIBUTION/AVAILABILITY CODES	
Dist.	AVAIL. and/or SPECIAL
A	

DDC  
RECEIVED  
DEC 6 1977  
D

## LIST OF FIGURES

Figure		Page
2.1-1	Model of Radar Signal Processing	4
2.3-1	Matched Filter Receiver	9
3.4-1	Barker Code (a) plot of code (b) associated autocorrelation function	20
3.5-1	Root Structure of $S(z)$	23
3.5-2	Huffman Code (a) plot of code (b) associated autocorrelation function	25
4.3-1	Cascade Configuration for Generation of Autocorrelation Sequence	31
5.1-1	Pseudo-Optimum (a) plot of code (b) associated autocorrelation function	39
5.1-2a	Plot of $ \chi(\tau, \omega) $ for the Pseudo-Optimum Code of Length 11	40
5.1-2b	Plot of $ \chi(\tau, \omega) $ for the Huffman Code of Length 11	40
5.1-2c	Plot of $ \chi(\tau, \omega) $ for the Barker Code of Length 11	41
5.2-1	Pseudo-Optimum Code of length 128 (a) magnitude of code $ \mu(t) $ (b) corresponding autocorrelation function $R_{\mu}(\tau)$	43
5.2-1	Plot of Ambiguity Function Magnitude $ \chi(\tau, \omega) $ for the Pseudo-Optimum Code of Length 128	44

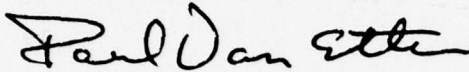
LIST OF TABLES

Table		Page
3.4-1	Barker Codes	19
4.4-1	Basic Steps on Linearization Algorithm	35
5.1-1	Initial Code Selection-Length 11	38
5.2-1	Relevant Characteristics of Real Pulse-Burst Codes of Length 128	42



## EVALUATION

This report describes the research accomplished between 1 June 1977 and 1 August 1977. The significance of this report is that a new pulse burst waveform is presented that obtains lower time side lobes than any other previously known waveforms. The new pulse burst waveform is compared with the well known Barker and Hoffman codes.



Paul VanEtten  
Project Engineer

## SECTION 1

### INTRODUCTION

#### 1.1 PURPOSE

This report describes some initial results in the algorithmic generation of finite length pulse burst signals whose autocorrelation functions are approximately impulse-like in nature. The codes will be restricted to be real with piecewise constant amplitude that can either be positive or negative (i.e., bi-phase). Such codes find various applications in radar signal processing and digital communication systems.

#### 1.2 BACKGROUND

In pulsed radar systems where it is required to improve upon the probability of target detection for a given false alarm rate, it is necessary to increase the transmitted pulse's energy level. Ideally the transmitted pulse should have a very small time-duration and large amplitude in order to achieve a high probability of detection while maintaining acceptably good range resolution characteristics. Unfortunately, since all radar transmitters have a peak power limitation of some sort, it is not possible to arbitrarily increase the transmitted pulse's amplitude. To raise the energy of transmission, it is then necessary to increase the pulse's time-duration. This will typically have a detrimental effect, however, on the resultant range resolution and ambiguity function characteristics.

There exists a class of techniques, generally referred to as pulse compression methods, that overcome the above mentioned inherent pitfall which large time-width pulses are susceptible to. In particular, by appropriate signal processing (e.g., matched filtering), it is possible to achieve the effect of a short time duration-large amplitude pulse while actually transmitting a relatively long time duration-moderate amplitude pulse. Two of the most widely studied of pulse compression methods are linear frequency modulating pulse compression, and, pulse burst signals (e.g., see ref. [6]). In this report, we will be concerned with presenting an algorithmic method for synthesizing pulse burst signals whose associated autocorrelation function approximates the ideal spike-like time-behavior which is the goal of many radar system designs.

## SECTION 2

### RADAR SIGNAL DESCRIPTION

#### 2.1 BASIC SIGNAL MODEL

In radar target detection and tracking applications, the return signal from a target is often modeled as a simple transformed version of the transmitted signal. If the target is taken to be a moving point in space, then the return signal  $r(t)$  is usually related to the transmitted signal  $s(t)$  based on the following two hypotheses.

- (i) the return signal will be a time delayed version of the transmitted signal (i.e.,  $r(t) = s(t-\tau)$ ) where  $\tau$  is proportional to the distance between the target and the transmitting radar.
- (ii) there will be imposed a frequency shift of  $\omega_d$  on the transmitted signal's spectrum which is proportional to the target's radial velocity relative to the radar system (i.e.,  $R(\omega) = S(\omega - \omega_d)$ ). The quantity  $\omega_d$  is referred to as the Doppler shift and is positive for targets moving toward the radar system.

The combined effect of these two factors will then characterize the return signal from a point target moving at a constant range rate. It is tacitly assumed in this model that the transmitted signal is narrow band and that the target's range rate is much less than the speed of light.

To demonstrate the implications of this signal model, let us consider the important case in which the transmitted signal is a modulated sinusoid, that is

$$s(t) = a(t) \cos[\omega_0 t + \theta(t)] \quad (2.1-1)$$

where  $a(t)$  and  $\theta(t)$  are the real envelope and phase modulating signals, respectively, while  $\omega_0$  is the associated carrier frequency. Generally, these two modulating signals vary slowly in time relative to the unmodulated carrier signal  $\cos[\omega_0 t]$ . According to the return signal model as specified by the above hypotheses, it follows that the associated return signal (in the

absence of noise) from a perfectly reflecting point target will be of the form

$$r(t) = a(t-\tau) \cos[(\omega_o + \omega_d)(t-\tau) + \theta(t-\tau)] \quad (2.1-2)$$

where  $\tau$  and  $\omega_d$  correspond to the target's range and range rate, respectively. Once the values of  $\tau$  and  $\omega_d$  are determined, the point target's range and radial range rate are found from the relationships

$$R = c\tau/2, \quad \dot{R} = c\omega_d/2\omega_o$$

where  $c$  denotes the velocity of light.

Although expression (2.1-2) yields a generally good model for the deterministic component of the return signal from a point target, it must be appreciated that the actual return signal will be contaminated by additive noise. A more realistic return signal model will be then given by

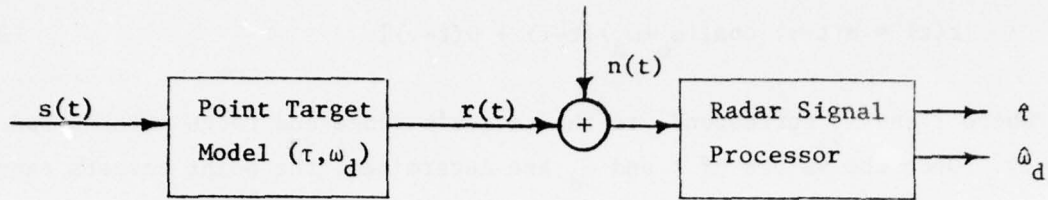
$$\begin{aligned} x(t) &= r(t) + n(t) \\ &= a(t-\tau) \cos[(\omega_o + \omega_d)(t-\tau) + \theta(t-\tau)] + n(t) \end{aligned}$$

where  $n(t)$  denotes a nondeterministic noise signal which can arise from such sources as atmospheric conditions, clutter, chaff, etc. The main objective of radar signal processing is that of processing this noise contaminated signal so as to obtain an appropriately accurate estimation of the delay-Doppler shift pair  $(\tau, \omega_d)$ . As might be anticipated, this estimation will be considerably enhanced if the modulating signals  $a(t)$  and  $\theta(t)$  are judiciously chosen.

It will be beneficial to depict the radar signal processing model as shown in Figure 2.1-1. The transmitted signal  $s(t)$  is shown as being operated upon to produce the corresponding point return signal model  $r(t)$  which in turn has added to it the nondeterministic noise signal  $n(t)$ . This sum signal is then operated upon by a radar signal processor to generate esti-



mates  $(\hat{\tau}, \hat{\omega}_d)$  of the target's actual delay-Doppler shift parameters  $(\tau, \omega_d)$ .



$$s(t) = a(t) \cos[\omega_0 t]$$

$$r(t) = a(t-\tau) \cos[(\omega_0 + \omega_d)(t-\tau) + \theta(t-\tau)]$$

FIGURE 2.1-1 MODEL OF RADAR SIGNAL PROCESSING

## 2.2 TARGET RESOLUTION AND THE AMBIGUITY FUNCTION

One of the primary tasks of a radar signal processor is that of detecting the presence of (or resolving) two or more targets in the return signal. As is well known, this capability is very much dependent on the selection of the envelope and phase modulating signals  $a(t)$  and  $\theta(t)$ , respectively of the transmitted signal. This is readily made apparent by considering the special case in which there are two point targets in space that have the associated delay-Doppler shift pairs  $(\tau_1, \omega_1)$  and  $(\tau_1 + \tau, \omega_1 + \omega)$ . The two targets are then said to be separated by the differential delay  $\tau$  and differential Doppler shift  $\omega$ . Using the previous section's postulated point target model, it follows that the noise free return signal from each of these point targets will be

$$r_1(t) = a(t-\tau_1) \cos[(\omega_0 + \omega_1)(t-\tau_1) + \theta(t-\tau_1)] \quad (2.2-1a)$$

and

$$r_2(t) = a(t-\tau_1-\tau) \cos[(\omega_0 + \omega_1 + \omega)(t-\tau_1-\tau) + \theta(t-\tau_1-\tau)] \quad (2.2-1b)$$

The ability to resolve these two point target return signals will be obviously dependent upon the distinctiveness of their timewise behavior. There are a variety of measures for quantizing this timewise distinctiveness. Undoubtably, the most widely used such measure is the integral of the difference squared (integral squared error) as given by

$$E(\tau, \omega) = \int_{-\infty}^{\infty} [r_1(t) - r_2(t)]^2 dt \quad (2.2-2)$$

This integral squared error criterion yields a very effective means for gauging the distinctiveness of two point target return signals. In addition, its utilization leads to a desirable and tractable analysis.

The modulating signals  $a(t)$  and  $\theta(t)$  are said to readily resolve the two point target return signals (2.2-1) with differential delay-Doppler shift pair  $(\tau, \omega)$ , if the integral squared error (2.2-2) takes on a suitably large positive value. It is clear that this criterion will be zero at  $\tau=0, \omega=0$  since the return signals  $r_1(t)$  and  $r_2(t)$  are identical in that case. Our basic objectives in selecting  $a(t)$  and  $\theta(t)$  will be that of causing this integral squared error measure to be large positive for delay-Doppler shift pairs not at the origin of the  $(\tau, \omega)$  plane.

To evaluate the postulated integral squared error criterion, one simply substitutes the point target return signal expressions (2.2-1) into relationship (2.2-2). Utilizing simple trigonometric identities and the assumption that the modulating signals  $a(t)$  and  $\theta(t)$  are slowly varying time signals relative to the unmodulated signal  $\cos[\omega_0 t]$ ,<sup>1</sup> it is readily shown

<sup>1</sup>This is commonly referred to as the "narrow band signal" assumption and is typical of most radar signals. In essence, the narrow band signal assumption sets to zero all integrals of the form

$$\int_{t_0}^{t_1} x(t) \sin[\omega_0 t + \theta] dt$$

where the signal  $x(t)$  is a very slowly varying function of time relative to the sinusoidal signal  $\sin[\omega_0 t + \theta]$ .

that the integral squared error criterion is given by (e.g., see ref [2])

$$E(\tau, \omega) = \int_{-\infty}^{\infty} a^2(t) dt - |\chi(\tau, \omega)| \cos[(\omega_0 + \omega_1 + \omega)\tau + \angle \chi(\tau, \omega)] \quad (2.2-3)$$

The complex valued function  $\chi(\tau, \omega)$  which appears in this expression is known as the "ambiguity function" which corresponds to the transmitted signal and is formally given by

$$\chi(\tau, \omega) = \int_{-\infty}^{\infty} \mu(t) \mu^*(t-\tau) e^{-j\omega t} dt \quad (2.2-4)$$

where  $\mu(t)$  is the so-called complex valued modulating signal specified by

$$\mu(t) = a(t) e^{j\theta(t)} \quad (2.2-5)$$

This complex modulating signal will play a major role in much of what is to follow. It is seen to be uniquely specified by the transmitted signal's modulating envelope and phase signals.

An inspection of the above closed-form expression for  $E(\tau, \omega)$  reveals that the second term is the only one dependent on the differential delay-Doppler shift pair  $(\tau, \omega)$ . Furthermore, for virtually all radar signals of interest, the ambiguity function  $\chi(\tau, \omega)$  will be a much slower varying function of  $\tau$  than will its multiplicative cosine term. With this in mind, it then follows that if one desires  $E(\tau, \omega)$  to be as large as possible for a continuous range of differential delay  $\tau$  values, it is necessary that the quantity  $|\chi(\tau, \omega)|$  which multiplies the rapidly varying cosine term must be near zero for all values of  $(\tau, \omega)$  other than the origin.

Thus, an ideal ambiguity function would be one which is everywhere zero in the  $(\tau, \omega)$  plane except at the origin where it has value equal to the energy in the signal  $a(t)$ , that is

$$\chi(\tau, \omega)_{\text{ideal}} = \begin{cases} \int_{-\infty}^{\infty} a^2(t) dt & \tau = \omega = 0 \\ 0 & \text{otherwise} \end{cases}$$

Although it is impossible to generate a physically realizable set of modulating signals  $a(t)$  and  $\theta(t)$  which will attain this ideal objective, this behavior will serve as a comparison reference for judging the worth of practical modulating signals in resolving multiple targets. In summary a good modulation signal selection  $\mu(t) = a(t)e^{j\theta(t)}$  is one whose corresponding ambiguity function closely approximates this spike-like behavior.

The ambiguity function as defined by relationship (2.2-4) possesses a number of interesting analytical properties which will characterize its behavior in the  $(\tau, \omega)$  plane. Some of the more basic properties are:

$$\text{Property 1} \quad \chi(0,0) = \int_{-\infty}^{\infty} a^2(t)dt \geq |\chi(\tau, \omega)|$$

$$\text{Property 2} \quad \frac{1}{2\pi} \int_{-\infty}^{\infty} \int_{-\infty}^{\infty} |\chi(\tau, \omega)|^2 d\tau d\omega = \chi^2(0,0)$$

$$\text{Property 3} \quad |\chi(\tau, \omega)| = |\chi(-\tau, -\omega)|$$

Property 2 is particularly noteworthy in that it indicates that the postulated ideal ambiguity function is not achievable. Namely, since the volume under the  $|\chi(\tau, \omega)|^2$  surface is a constant, any attempt to cause  $|\chi(\tau, \omega)|$  to be spike-like will invariably result in a large spread of nonzero levels off the origin.

### 2.3 THE MATCHED FILTER

One of the primary objectives of any radar signal processor is that of detecting the existence of a weak return signal in the presence of additive noise. This detection will be enhanced if the linear processor's unit-impulse response is chosen to in some sense match the return signals waveform. To illustrate this concept, let us consider the specific case in which the input is given by

$$x(t) = r(t) + n(t)$$

where  $r(t)$  denotes the useful return signal component and  $n(t)$  is additive



noise. If the additive noise is white, it is well-known that the "matched filter" whose unit-impulse response is specified by

$$h(t) = r^*(-t) \quad (2.3-1)$$

will maximize the output signal-to-noise power ratio at time  $t=0$ .<sup>1</sup> A linear filter with this unit-impulse response is then said to be optimally matched for detecting the signal  $r(t)$  which is masked by additive white noise. Similar results may be obtained when the additive noise is other than white (e.g., see ref. [2]).

With this in mind, let us consider the typical matched filter receiver shown in Figure 2.3-1 in which the input signal is taken to be of the form

$$r(t) = a(t-\tau) \cos[(\omega_0 + \omega)(t-\tau) + \theta(t-\tau)] \quad (2.3-2)$$

and where the delay-Doppler shift pair  $(\tau, \omega)$  is not known apriori. It will be assumed that the matched filter was designed to detect the presence of a return signal whose Doppler shift is  $\omega_1$ . The unit-impulse response of the required matched filter is readily found to be

$$h(t) = a(-t) \cos[(\omega_0 - \omega_a + \omega_1)t - \theta(-t)] \quad (2.3-3)$$

It can be shown that the response of this matched filter to input signal (2.3-2) is given by

$$y_c(t) = \frac{1}{4} |\chi(\tau-t, \omega-\omega_1)| \cos[(\omega_0 - \omega_a + \omega)t + \angle \chi(\tau-t, \omega-\omega_1)]$$

where  $\chi(\tau, \omega)$  is the ambiguity function corresponding to the complexed valued

<sup>1</sup>Generally, for purposes of physical realizability, the required matched filter's unit-impulse response must be appropriately time shifted for causal signal processing (i.e.,  $r^*(T_0 - t)$ ). In this case, the output signal to noise power ratio is maximized at  $t=T_0$ .

modulating signal  $\mu(t) = a(t)e^{j\theta(t)}$ . In arriving at this result, the narrow-band signal assumption is made in which the intermediate frequency  $\omega_o - \omega_a$  is taken to be very large.

Thus, the signal processor's output is seen to have an envelope which is equal to a translated version of the transmitted signal's associated ambiguity function magnitude. If the matched filter is "tuned" to the input signal (i.e.,  $\omega_1 = \omega$ ), then the envelope of the output signal will peak at time  $t=\tau$  thereby indicating the presence of a target at the range corresponding to delay  $\tau$ . This particular form of matched signal processing has served as a very effective means for detecting the presence of weak target return signals in a background of strong noise. Namely, one looks for the presence of pulse like peaks in the envelope and measures the times at which they occur. From the above remarks, it is apparent that the ambiguity function takes on added meaning whenever matched filtering operations are utilized.

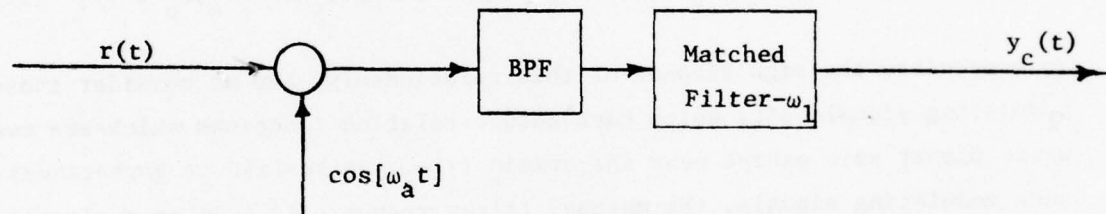


FIGURE 2.3-1 MATCHED FILTER RECEIVER

#### 2.4 AUTOCORRELATION FUNCTION

The ability to achieve fine range measurements is inherently linked to the time behavior of the autocorrelation function which is associated with the modulating signal. This is readily demonstrated by noting that the envelope of the response of matched filter (2.3-3) to the input signal

given by expression (2.3-2) with  $\omega = \omega_1$  is simply

$$y_e(t) = \frac{1}{4} |\chi(\tau-t, 0)| \quad (2.4-1)$$

The ambiguity function evaluated at  $\omega=0$  is otherwise known as the autocorrelation function associated with  $\mu(t)$  and is formally defined by

$$R_\mu(\tau) = \chi(\tau, 0) = \int_{-\infty}^{\infty} \mu(t) \mu^*(t-\tau) dt \quad (2.4-2)$$

The value of this autocorrelation function at  $\tau=0$  is seen to be equal to the energy contained in the modulating signal. It is a well-known fact that the autocorrelation function's magnitude is maximum at  $\tau=0$  (i.e.,  $R_\mu(0) \geq |R_\mu(\tau)|$  for all  $\tau$ ).

In summary, we have established the following very important input-response pair relationship for the matched filter operator (2.3-3)

$$x(t) = a(t-\tau) \cos[(\omega_0 + \omega_1)(t-\tau) + \theta(t-\tau)] \Rightarrow y_e(t) = \frac{1}{4} |R_\mu(t-\tau)| \quad (2.4-3)$$

To appreciate the significance of this relationship, let us consider those modulating signals  $\mu(t)$  which have autocorrelation functions which are everywhere almost zero except near the origin (i.e., spike-like in appearance). For such modulating signals, the matched filter response (2.4-3) is a signal which is everywhere zero except near  $t=\tau$  where a spike will appear. Thus, to detect the presence of target echoes in the return signal, one would simply examine the matched filter's response signal for the existence of spikes. The existence of a spike would indicate the presence of a target whose range is proportional to the time occurrence of that spike. Clearly, the narrower the width of the spike, the more precisely the target's range can be determined.

With the above thoughts in mind, it is apparent that the class of modulating signals which have impulse-like autocorrelation functions are of great usefulness in radar signal processing. The ideal autocorrelation function would be one for which  $R_\mu(t)$  is identically zero except at  $\tau=0$  where its

value equals the energy in the modulating signal. Although this ideal objective cannot be achieved by physically realizable modulating signals, it serves as a basis for comparing the effectiveness of different modulating signals.



## SECTION 3

### PULSE-BURST SIGNALS

#### 3.1 BASIC DEFINITIONS

A particularly effective method for generating radar signals which possess desirable fine range resolution characteristics is that of pulsed sinusoidal modulation. In general, a pulsed sinusoid consists of a clustered sequence of  $L+1$  sinusoid signals each of duration  $T$  seconds. In each of these  $L+1$  "inner-pulse" intervals, the sinusoid's amplitude and phase angle will be held fixed, but, these parameters will generally vary from one inner-pulse interval to the next. Signals so characterized are commonly referred to as "pulse-burst signals" and have the following convenient analytical representation

$$s(t) = \sum_{k=0}^L a_k \cos[\omega_0 t + \theta_k] \{u(t-kT) - u(t-kT-T)\} \quad (3.1-1)$$

where  $a_k$  and  $\theta_k$  designate the transmitted sinusoid's amplitude and phase angle, respectively, during the  $k^{\text{th}}$  inner pulse interval  $kT \leq t < kT+T$  and  $u(t)$  denotes the standard unit-step signal.<sup>1</sup> This pulse-burst signal is seen to have a time duration of  $LT+T$  seconds and is identically zero outside the time interval  $0 \leq t < LT+T$ . We shall refer to this pulse burst signal as having length  $L+1$  and its time behavior is seen to be completely specified by the  $2L+2$  real numbers  $\{a_0, a_1, \dots, a_L\}$  and  $\{\theta_0, \theta_1, \dots, \theta_L\}$ .

In order to determine the suitability of this signal for radar processing applications, let us first obtain the complex modulating signal  $\mu(t)$  which corresponds to it. According to expressions (2.1-1) and (2.2-5), this complex modulating signal is specified by the following piecewise constant function of time

<sup>1</sup>The unit-step signal is defined by

$$u(t) = \begin{cases} 1 & t > 0 \\ 0 & t < 0 \end{cases}$$

$$\mu(t) = \sum_{k=0}^L a_k e^{j\theta_k} \{u(t-kT) - u(t-kT-T)\} \quad (3.1-2)$$

Again, it is clear that magnitude and phase angle parameters  $\{a_k\}$  and  $\{\theta_k\}$  play a major role in characterizing the underlying radar signal. In particular, the associated ambiguity function (2.2-4) which depicts the desirability of the transmitted signal for radar processing is seen to be explicitly dependent on  $\mu(t)$  and therefore on these parameters.

#### PULSE-BURST CODE

The suitability of a given pulse-burst signal for radar processing is then completely determined by the selection of the  $L+1$  complex numbers

$$\mu_k = a_k e^{j\theta_k} \quad \text{for } k = 0, 1, \dots, L \quad (3.1-3)$$

It is clear that a knowledge of these  $\mu_k$  elements uniquely identifies the pulse-burst signal (3.1-1) and vice-versa. As such, the finite sequence

$$\{\mu_0, \mu_1, \dots, \mu_L\} \quad (3.1-4)$$

will be referred to as the "pulse burst code" associated with the pulse burst signal (3.1-1). In much of what is to follow, we will be concerned with presenting (or developing) methods for selecting the code elements  $\mu_k$  so that the autocorrelation function associated with the complex modulating signal  $\mu(t)$  takes on desirable characteristics.

#### AMBIGUITY FUNCTION OF A PULSE-BURST SIGNAL

It has been previously indicated that the ambiguity function associated with a given complex modulating signal provides an attractive visual method for judging a signal's effectiveness in radar processing. With this in mind, the ambiguity function which corresponds to pulse burst signal (3.1-1) was next found and is given by

$$\chi(nT+\Delta, \omega) = (T-\Delta)e^{\frac{j\omega(T-\Delta)}{2}} \operatorname{sinc}\left[\frac{\omega(T-\Delta)}{2}\right] \sum_{k=n}^L \mu_k \mu_{k-n}^* e^{-j\omega kT} + \quad (3.1-5)$$

$$\Delta e^{\frac{j\omega(2T-\Delta)}{2}} \operatorname{sinc}\left[\frac{\omega\Delta}{2}\right] \sum_{k=n+1}^L \mu_k \mu_{k-n-1}^* e^{-j\omega kT}$$

for  $n = 0, \pm 1, \pm 2, \pm 3, \dots$  and  $0 \leq \Delta < T$

An examination of this ambiguity expression indicates two interesting characteristics of pulse-burst signals. First of all, this ambiguity function is identically zero for delays greater than the pulse-burst length  $LT+T$  (i.e.,  $|n| > L$ ). Furthermore, since the two summations in this relationship are each periodic functions of  $\omega$  with period  $2\pi/T$ , it follows that the ambiguity function will tend to periodically decay to zero in a  $\sin x/x$  manner in the  $\omega$  direction for a fixed delay time.

Once the values for the pulse code  $\mu_0, \mu_1, \dots, \mu_L$  have been assigned, it is a simple matter to generate the surface behavior of the ambiguity function (3.1-5) with the aid of a suitable computer program and plotting routine (e.g., see Appendix 8.1). In addition, with the use of this convenient expression, the distinct possibility exists that one may generate an algorithmic procedure for selecting the code elements  $\mu_k$  so that the ambiguity function will be optimum in some sense (e.g., impulse-like in behavior). This will be demonstrated, to some extent, in the next section when these code elements are chosen to make the associated autocorrelation function impulse-like.

### 3.2 AUTOCORRELATION OF A PULSE-BURST SIGNAL

As indicated in Section 2.4, an important objective in many radar signal processing applications is the generation of finite duration modulating signals whose autocorrelation is impulse-like. The autocorrelation function which corresponds to a pulse burst signal is readily obtained by evaluating the associated ambiguity function (3.1-5) at  $\omega=0$  to yield

$$R_{\mu}(nT+\Delta) = (T-\Delta) \sum_{k=n}^L \mu_k \mu_{k-n}^* + \Delta \sum_{k=n+1}^L \mu_k \mu_{k-n-1}^* \quad (3.2-1)$$

$$n = 0, \pm 1, \pm 2, \dots \text{ and } 0 \leq \Delta < T$$

From this expression, it is apparent that this autocorrelation function  $R_{\mu}(\tau)$  is identically zero outside the interval  $|\tau| \leq LT+T$ . This is an obvious consequence of the fact that the duration of the modulating signal  $\mu(t)$  is  $LT+T$  seconds.

It will be desirable to investigate this autocorrelation function at integral multiple values of  $T$  seconds (i.e.,  $\Delta=0$ ). This yields the sampled autocorrelation sequence

$$R_{\mu}(nT) = T \sum_{k=n}^L \mu_k \mu_{k-n}^* \quad (3.2-2)$$

whose elements are identically zero for integer values  $n$  satisfying  $|n| > L$ . It is possible to reconstruct the original autocorrelation function (3.2-1) from this associated sampled autocorrelation function by means of the simple relationship

$$R_{\mu}(nT+\Delta) = (1-\Delta)R_{\mu}(nT) + \Delta R_{\mu}(nT+T) \quad \text{for } 0 \leq \Delta < T$$

This is observed to be a straight line interpolation between the sampled values. Thus, pulse-burst signals as represented by modulating signal (3.1-2) will have associated autocorrelation functions which are piecewise linear and continuous.

### 3.3 QUALITY MEASURES OF A PULSE-BURST SIGNAL

The code sequence  $\mu_0, \mu_1, \dots, \mu_L$  which corresponds to a pulse-burst signal is said to possess an impulse-like autocorrelation if the sampled autocorrelation is such that the normalized maximum side lobe as defined by

$$\lambda = \max_{n \neq 0} \frac{|R_{\mu}(nT)|}{R_{\mu}(0)} \quad (3.3-1)$$



is sufficiently close to zero (note,  $0 \leq \lambda \leq 1$ ). In other words, the zero<sup>th</sup> element of an impulse-like sampled autocorrelation sequence dominates the magnitude of its remaining elements. A variety of systematic procedures for selecting the code sequence  $\mu_0, \mu_1, \dots, \mu_L$  have been developed for achieving such autocorrelation function behavior. Before presenting two of the more popular of such methods, let us first outline some practical considerations which are imposed on pulse-burst signals.

In order to achieve satisfactory probability of detection for a given false alarm rate, it is necessary that sufficient signal energy be transmitted. For pulse-burst signals, the transmitted signal's energy is equal to one half the energy in the modulating signal  $\mu(t)$ . The modulated signals energy, however, is simply equal to  $R_\mu(0)$ , that is

$$E_\mu^2 = T \sum_{k=0}^L \mu_k \mu_k^* \quad (3.3-2)$$

This quantity must be made larger than some prescribed value in order to obtain a satisfactory probability of detection for a given false alarm rate. There are three methods for increasing the modulating signal's energy

- (i) increase the inner-pulse duration time  $T$
- (ii) increase the magnitude of the code elements  $\mu_k$
- (iii) increase the length of the pulse code

Since the main spike of the pulse-burst autocorrelation function is defined over the time interval  $-T \leq t \leq T$ , fine range resolution considerations restrict the size of the inner-pulse duration time  $T$ . Furthermore, peak power limitations of the radar transmitter restrict the magnitude of the individual code elements to be no larger than a fixed quantity. With this in mind, it follows that the most practical method for increasing the energy of the transmitted signal is to increase the code length and to simultaneously have each of the code element values  $\mu_k$  be nearly equal in magnitude (i.e., peak power is nearly maintained throughout the burst).

In selecting the elements  $\mu_0, \mu_1, \dots, \mu_L$  of a pulse-burst code, we

will then be concerned with both obtaining an autocorrelation function which is impulse-like while simultaneously maintaining a reasonably efficient means of transmitting signal energy. A criterion which measures this last criterion is the so-called energy efficiency as defined by [5]

$$\rho = \frac{\text{burst signal energy transmitted}}{\text{energy transmitted at peak power over each } T \text{ second duration}} \quad (3.3-3)$$

$$= \frac{\sum_{k=0}^L |\mu_k|^2}{(L+1)(\max |\mu_k|^2)} = \frac{E_\mu}{(L+1)(\max |\mu_k|^2)}$$

This criterion takes on values in the interval  $0 \leq \rho \leq 1$  with the most energy efficient codes being those with equal code magnitude and  $\rho=1$ . To measure a codes variance from the most efficient energy mode (i.e.,  $\rho=1$ ), the following criterion has been also used [5]

$$\epsilon = \frac{1}{L+1} \sum_{k=0}^L \left\{ |\mu_k| - \frac{E_\mu}{L+1} \right\}^2 \quad (3.3-4)$$

Although a given pulse-burst code may possess an autocorrelation function which is impulse-like, it may be deemed unsatisfactory if its energy efficiency is too small. A truly good pulse-burst code is one whose individual elements are nearly equal in magnitude and which has an impulse-like autocorrelation function. The Barker codes to be presented in the next section are an example of such a code.

#### 3.4 CONSTANT MAGNITUDE CODES

When transmitting a pulsed-sinusoidal signal under amplitude constraints, maximum power transmittal is achieved by maintaining a maximum sinusoid amplitude. In terms of a pulse-burst code, this corresponds to having the elements of the code be specified by

$$\mu_k = Ae^{j\theta_k} \quad k = 0, 1, \dots, L \quad (3.4-1)$$

where  $A$  corresponds to the peak amplitude limitation. The energy utilization efficiency for a code of this nature is optimum (i.e.,  $\rho=1$ ) and its variance is likewise minimal (i.e.,  $\epsilon=0$ ). We shall refer to a code whose elements are specified by relationship (3.4-1) as a constant magnitude code to reflect the fact that  $|\mu_k|=A$  for  $k = 0, 1, 2, \dots, L$ .

In synthesizing a constant magnitude code, one seeks to select the phase terms  $\theta_0, \theta_1, \dots, \theta_L$  so that the resultant transmitted signal has an associated autocorrelation function which is near impulse-like in behavior. The autocorrelation sequence which corresponds to code (3.4-1) is readily obtained by utilization of expression (3.2-2) and results in

$$R_{\mu}(nT) = A^2 T \sum_{k=n}^L e^{j[\theta_k - \theta_{k-n}]} \quad n = 0, 1, \dots, L \quad (3.4-2)$$

#### BINARY CODES AND THE BARKER CODES

One of the most widely studied of constant magnitude codes are those for which the phase angle elements  $\theta_k$  take on the exclusive values of 0 or  $\pi$ . Such codes are also called binary codes in that the code elements  $\mu_k$  take on either of the two real values  $A$  or  $-A$ . Binary codes are of interest mainly because of their optimum energy utilization efficiency, and, the ease with which they may be generated.

To illustrate a particular important class of binary codes, let us now consider the Barker codes. The code  $\{\mu_0, \mu_1, \mu_2, \dots, \mu_L\}$  is said to be Barker if its elements are exclusively plus or minus one and its associated autocorrelation sequence is specified by

$$R_{\mu}(nT) = \begin{cases} L+1 & n = 0 \\ 0 \text{ or } \pm 1 & n \neq 0 \end{cases} \quad (3.4-3)$$

It is observed that the normalized maximum side lobe ratio for a Barker code is  $1/(L+1)$ . Thus, Barker codes would be ideal vehicles for obtaining impulse-like autocorrelation functions if the pulse-burst length  $L+1$  could be made suitably large. Unfortunately, Barker codes exist only for a small set of lengths as shown in Table 3.4-1. Thus, Barker codes have somewhat limited use and are generally not particularly appropriate in applications requiring

near impulse-like autocorrelation behavior.

Code Length	Code Elements
1	1
2	1, -1
3	1, 1, -1
4	1, 1, 1, -1
5	1, 1, 1, -1, 1
7	1, 1, 1, -1, -1, 1, -1
11	1, 1, 1, -1, -1, -1, 1, -1, -1, 1, -1
13	1, 1, 1, 1, 1, -1, -1, 1, 1, -1, 1, -1, 1

TABLE 3.4 -1

BARKER CODES

To illustrate the characteristics of a Barker code, let us consider the length 11 code as depicted in Figure 3.4-1. The autocorrelation function's magnitude which corresponds to this code is also shown along with the parameters characterizing the code's efficiency. In a later section, we will compare this code's characteristics with those of a so-called pseudo-optimum code generated by an algorithm to be presented in Section 4.



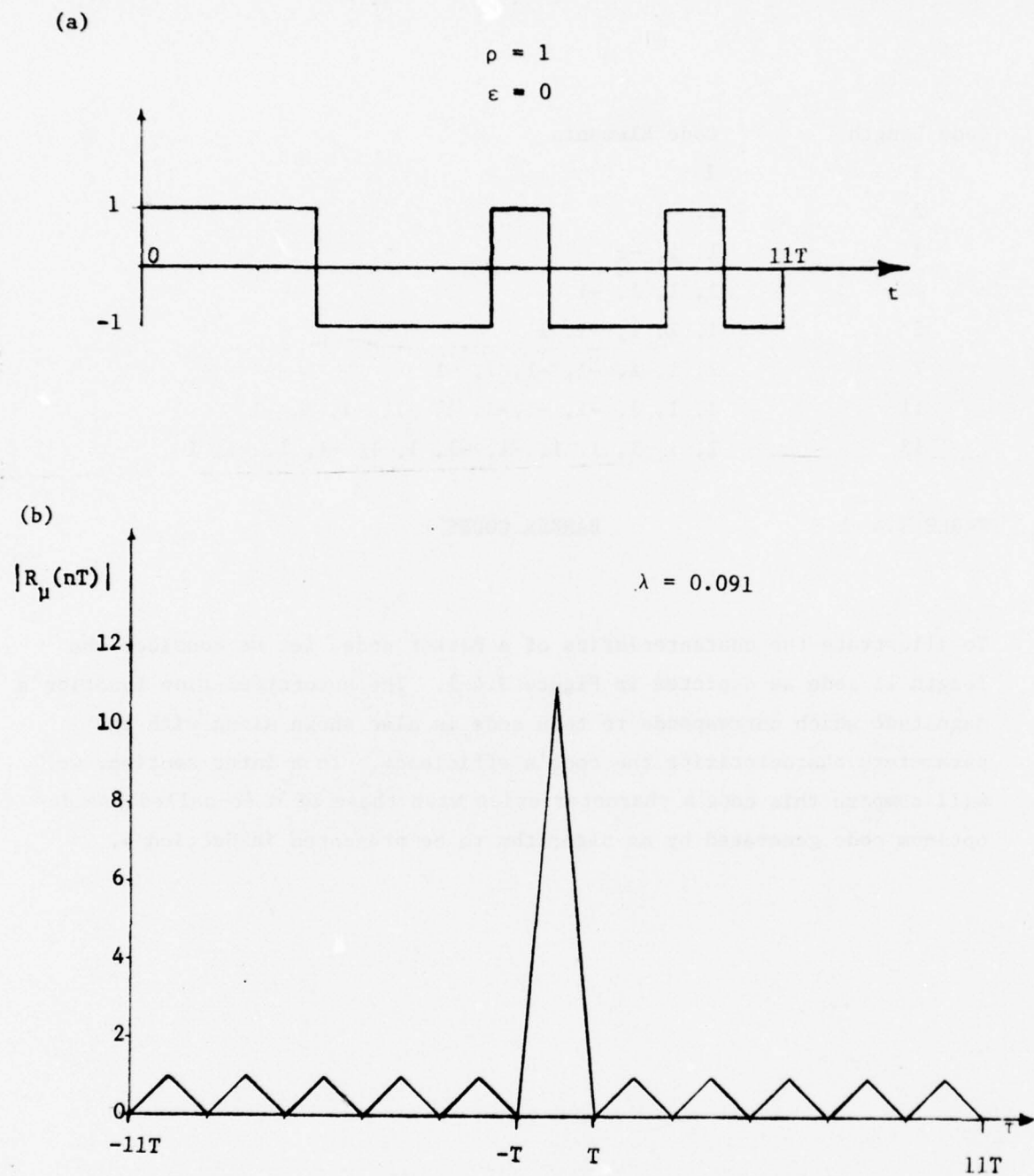


FIGURE 3.4-1 BARKER CODE (a) plot of code,  
(b) associated autocorrelation function

### 3.5 HUFFMAN CODES

In generating pulse-burst codes, superior impulse-like autocorrelation behavior can be achieved by allowing the code elements  $\mu_k$  to be unconstrained complex numbers. It is of course realized that in utilizing such codes, particular attention has to be paid to their associated energy utilization efficiency factor  $\rho$  when peak power limitations are imposed. The class of Huffman codes to be now considered offer an excellent example of high performance pulse-burst codes.

The generally complex valued code  $\{\mu_0, \mu_1, \dots, \mu_L\}$  is said to be a Huffman code if its associated autocorrelation sequence is given by

$$R_\mu(nT) = \begin{cases} E_\mu & n = 0 \\ -1 & n = \pm L \\ 0 & \text{otherwise} \end{cases} \quad (3.5-1)$$

where  $E_\mu = \sum |\mu_k|^2$  denotes the energy in the code sequence.<sup>1</sup> This autocorrelation sequence can be made more impulse-like by simply increasing the code's energy  $E_\mu$ . As a further observation, it is noted that the requirement  $R_\mu(LT) = \mu_0 \mu_L^* = -1$  imposes a constraint on the code's first and last element values.

In what is to follow, we shall be concerned with presenting a systematic procedure for selecting a  $L+1$  length complex code which will have the specified autocorrelation behavior (3.5-1). This is best begun by considering the  $z$ -transform of the finite length code  $\{\mu_k\}$  as defined by

$$P(z) = \mu_0 + \mu_1 z^{-1} + \mu_2 z^{-2} + \dots + \mu_L z^{-L} \quad (3.5-2)$$

where  $z$  is a complex variable. Noting that  $P(z)$  is a polynomial in the variable  $z^{-1}$ , it follows that the code transform has the equivalent factored representation

<sup>1</sup>The Huffman code in which  $R_\mu(LT) = e^{j\theta}$  can be synthesized in a manner similar to that to be presented in this section.

$$P(z) = \mu_0 z^{-L} (z-z_1)(z-z_2) \dots (z-z_L) \quad (3.5-3)$$

where  $z_k$  are the roots of  $P(z)$ . Clearly, if it is possible to determine, in some manner, the set of roots  $z_1, z_2, \dots, z_L$  of  $P(z)$  and the constant  $\mu_0$ , then one may generate the corresponding code elements by carrying out the indicated multiplications in expression (3.5-3). Such a procedure shall now be presented.

The  $z$ -transform of the autocorrelation sequence corresponding to the code  $\{\mu_0, \mu_1, \dots, \mu_L\}$  is readily found to be

$$\begin{aligned} S(z) &= \left[ \sum_{k=0}^L \mu_k z^{-k} \right] \left[ \sum_{n=0}^L \mu_n^* z^n \right] \\ &= -z^{-L} \left( \prod_{k=1}^L (z-z_k) \right) \left( \prod_{n=1}^L (z-1/z_n^*) \right) \end{aligned} \quad (3.5-4)$$

where use of the constraint  $\mu_0 \mu_L^* = -1$  has been made. It is seen that the roots of  $S(z)$  occur in reciprocal complex conjugate pairs with  $L$  of the roots belonging to  $P(z)$  and their corresponding  $L$  reciprocal complex conjugate pair mates belong to the polynomial multiplying  $P(z)$  in expression (3.5-4).

If a particular complex code sequence  $\{\mu_0, \mu_1, \dots, \mu_L\}$  is to have the specified autocorrelation sequence (3.5-1), these code elements must then be selected such that

$$S(z) = -z^{-L} (z^{2L-E_\mu} z^L + 1) \quad (3.5-5)$$

The polynomial  $z^{2L-E_\mu} z^L + 1$ , which in part constitutes the transform  $S(z)$ , is observed to be a mirror-image polynomial with real coefficients. It follows that if  $re^{j\theta}$  is a root of  $S(z)$ , then so must  $re^{j\theta}$ ,  $r^{-1}e^{j\theta}$ , and,  $r^{-1}e^{-j\theta}$  also be roots. Moreover, due to this basic structure, it is readily shown that the  $2L$  roots of  $S(z)$  are located at

$$re^{\frac{j2\pi k}{L}} \quad \text{and} \quad \frac{1}{r} e^{-\frac{j2\pi k}{L}} \quad k = 1, 2, \dots, L \quad (3.5-6)$$

where the scalar  $r$  is given by

$$r = \left[ \frac{1}{2} \left( E_{\mu} - \sqrt{E_{\mu}^2 - 4} \right) \right]^{1/L}$$

Thus, these  $2^L$  roots are seen to lie on two concentric circles centered at the origin along rays spaced every  $2\pi/L$  radians. This root pattern is depicted in Figure 3.5-1 for the special case  $N=8$ .

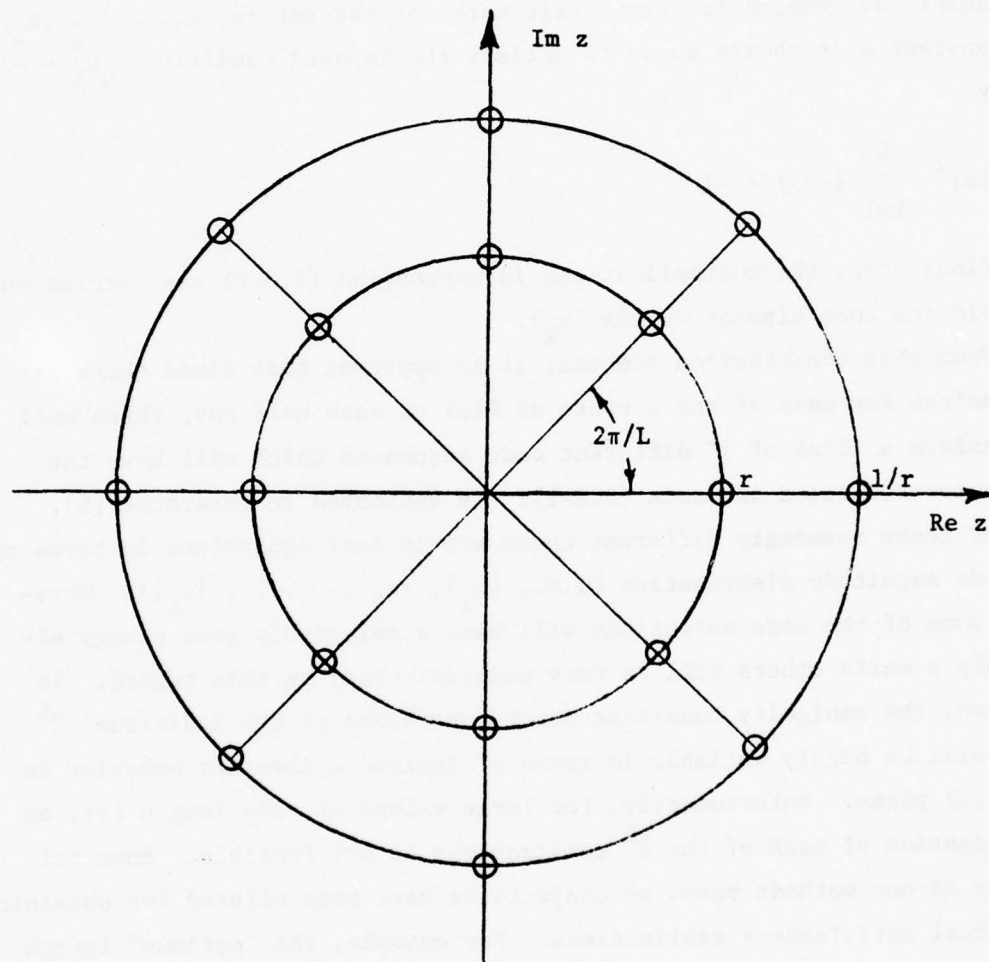


FIGURE 3.5-1

ROOT STRUCTURE OF  $S(z)$



To generate the roots of polynomial  $P(z)$ , one then simply selects  $z_k$  to be equal to either  $re^{j2\pi k/L}$  or  $r^{-1}e^{j2\pi k/L}$  for  $k = 1, 2, \dots, L$ . Carrying out this sequential root selection results in the following code transform

$$P(z) = \alpha z^{-L} (z-z_1)(z-z_2) \dots (z-z_L) \quad (3.5-7)$$

It is observed that the  $L$  roots not selected in this manner correspond to the reciprocal complex conjugate-pair mates of the set  $\{z_1, z_2, \dots, z_L\}$ . The constant  $\alpha$  is chosen so as to satisfy the imposed condition  $\mu_0 \mu_L^* = -1$ , namely

$$|\alpha|^2 \prod_{k=1}^L (-z_k) = -1$$

As a final step, the multiplications in expression (3.5-7) are carried out to yield the code element values  $\{\mu_k\}$ .

From this construction process, it is apparent that since there are two choices for each of the  $L$  roots of  $P(z)$  on each half ray, there will then exist a total of  $2^L$  different code sequences which will have the same autocorrelation sequence (3.5-1). As indicated in reference [5], some of these seemingly different codes are in fact equivalent in terms of the code magnitude distribution (i.e.,  $|\mu_1|, |\mu_2|, \dots, |\mu_L|$ ). Moreover, some of the code selections will have a relatively good energy efficiency  $\rho$  while others will be very unsatisfactory in this regard. In addition, the ambiguity functions which correspond to the individual  $2^L$  codes will be highly variable in terms of desired spike-like behavior in the  $(\tau, \omega)$  plane. Unfortunately, for large values of code length  $L+1$ , an investigation of each of the  $2^L$  realizations is not feasible. Some relatively ad-hoc methods based on conjectures have been offered for obtaining individual satisfactory realizations. For example, the "optimum" length 11 code in terms of energy efficiency is depicted in Figure 3.5-2 along with its associated autocorrelation function [5].

Before leaving the interesting subject of Huffman codes, let us

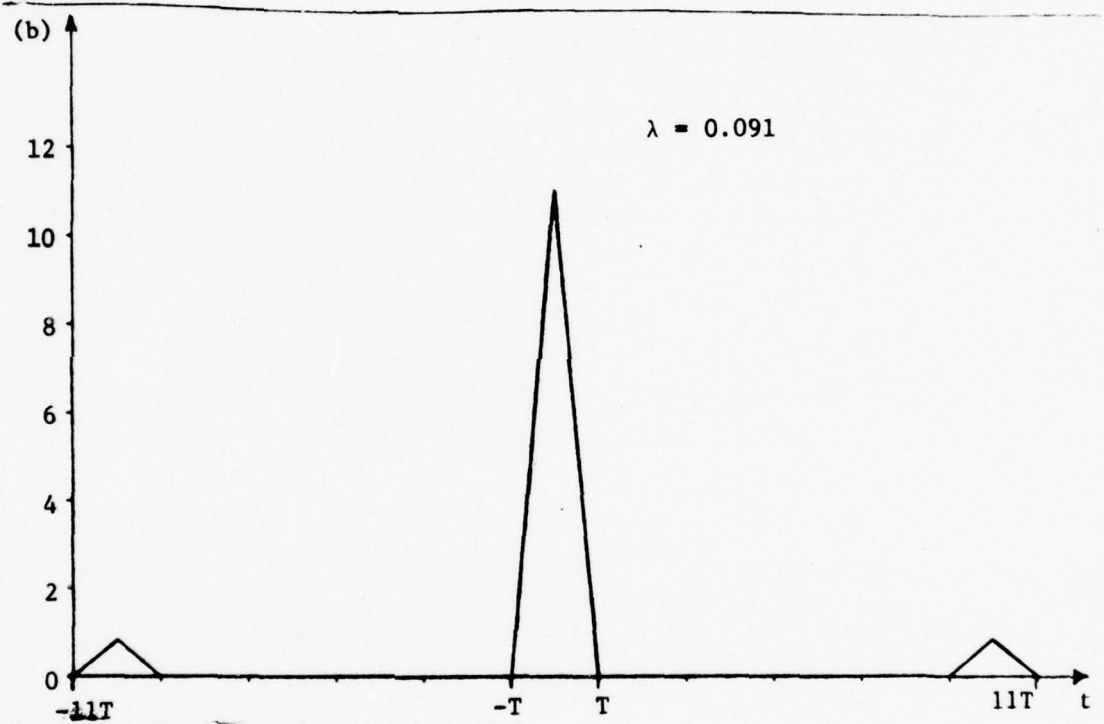
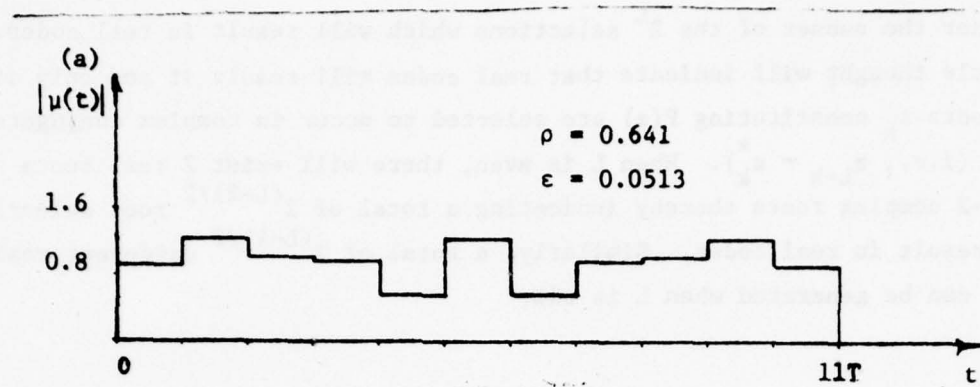


FIGURE 3.5-2 HUFFMAN CODE (a) plot of code,  
 (b) associated autocorrelation function

consider the subset of the  $2^L$  selections which will result in real codes. A little thought will indicate that real codes will result if and only if the roots  $z_k$  constituting  $P(z)$  are selected to occur in complex conjugate pairs (i.e.,  $z_{L-k} = z_k^*$ ). When  $L$  is even, there will exist 2 real roots and  $L-2$  complex roots thereby indicating a total of  $2^{(L-2)/2}$  root selections will result in real codes. Similarly, a total of  $2^{(L-1)/2}$  different real codes can be generated when  $L$  is odd.

## SECTION 4

### ALGORITHMIC GENERATION OF REAL PULSE-BURST CODES

#### 4.1 INTRODUCTION

In this section, we shall direct our attention exclusively to bi-phase codes in which the phase elements  $\theta_k$  are either 0 or  $\pi$ . A bi-phase code is typically referred to as a real burst code due to the fact that the associated complex modulating sequence  $\{\mu_0, \mu_1, \dots, \mu_L\}$  consists entirely of real numbers. It is to be noted that the Barker codes are real while a subset of Huffman codes are themselves real. Interest in real pulse-burst codes arises due to the simplicity of their generation as a modulated sinusoid since the only variable is the sinusoid's amplitude and not its phase.

#### 4.2 PSEUDO-OPTIMUM CODE

A pulse-burst code is said to be ideal if its associated sampled autocorrelation sequence is equal to

$$R_1(n) = E\delta(n) = \begin{cases} E & n=0 \\ 0 & n \neq 0 \end{cases} \quad (4.2-1)$$

in which  $\delta(n)$  designates the unit-Kronecker sequence and  $E$  denotes the code's energy<sup>1</sup>. It is not difficult to show that the only finite length codes which will have this characteristic are of length one. Unfortunately, length one codes are not of interest since the main purpose for using pulse-burst codes is that of transmitting a long duration pulse (to overcome peak power limitations) which in turn can be effectively transformed into a short duration pulse by means of a matched filtering operation. Although the above ideal autocorrelation behavior cannot be achieved by

<sup>1</sup>The unit Kronecker sequence is defined by

$$\delta(n) = \begin{cases} 0 & n=0 \\ 1 & n=\pm 1, \pm 2, \pm 3, \dots \end{cases}$$



a finite code of length greater than one, it can be closely approximated if the code elements are judiciously chosen. We shall now direct our attention to this most relevant task.

In what is to follow, we shall investigate the sampled autocorrelation sequence which corresponds to the  $L+1$  length real pulse-burst code  $\{\mu_0, \mu_1, \dots, \mu_L\}$ . In referring to the code as having length  $L+1$ , it is tacitly implied that its two end elements  $\mu_0$  and  $\mu_L$  need to be each nonzero for otherwise the code would be of a shorter length. To measure how closely this code's sampled autocorrelation sequence  $R_\mu(n)$  approximates the ideal objective (4.2-1), the standard squared error criterion will be used, that is

$$\begin{aligned} f(\mu) &= \sum_{n=-L}^L w(n) \{R_\mu(n) - R_i(n)\}^2 \\ &= w(0) \{R_\mu(0) - E\}^2 + 2 \sum_{n=1}^L w(n) R_\mu^2(n) \end{aligned} \quad (4.2-2)$$

The elements  $w(n)$  are nonnegative numbers which are used to weight the approximation errors in any desired manner. Due to the symmetry of the autocorrelation sequence, no loss of generality is introduced by assuming that  $w(-n) = w(n)$ . As a final observation, it is apparent from the formula for  $R_\mu(n)$  as given by

$$R_\mu(n) = \sum_{k=n}^L \mu_k \mu_{k-n}$$

that the above criterion  $f(\mu)$  is a quartic function of the code elements.

It is now desired to construct an acceptable code which will make this squared error criterion minimum. Unless a constraint of some form is imposed on this minimization, however, it is seen that an optimum code of length one will cause  $f(\mu)$  to take on the value zero (e.g.,  $\mu_0 = \sqrt{E}$ ,  $\mu_1 = \mu_2 = \dots = \mu_L = 0$ ). In order to avoid this possibility, we shall constrain the first code elements  $\mu_0$  to take on a fixed value  $\alpha$  and then

select the remaining  $L$  code elements to minimize criterion (4.2-2).<sup>1</sup> This constrained minimization problem is then expressed as

$$\min_{\{\mu_1, \mu_2, \dots, \mu_L\}} \left[ w(0) \left\{ \sum_{k=0}^L \mu_k^2 - E \right\}^2 + 2 \sum_{n=1}^L w(n) \left\{ \sum_{k=n}^L \mu_k \mu_{k-n} \right\}^2 \right] \quad (4.2-3)$$

where the analytic expression for  $R_\mu(n)$  has been incorporated. A code which renders this criterion a relative minimum value will be referred to as a "pseudo-optimum" code.

In order to encourage a uniform distribution of code power (i.e., each element has magnitude  $E/(L+1)$ ), a logical selection for the constant  $\alpha$  is  $E/(L+1)$ . It will be shown in section 5, however, that other selections will lead to superior codes. With this in mind, we shall let  $\mu_0$  take on various values and find the minimizing codes which correspond to each of these  $\mu_0$  selections. From this family of pseudo-optimum codes, we shall select one which is deemed to be superior (e.g., the one with maximum energy utilization efficiency).

A careful examination of criterion (4.2-3) indicates it to be a relatively highly nonlinear function of the code elements  $\mu_k$ . A closed-form solution for a minimizing code is then not feasible and one must appeal to an algorithmic solution approach. In the next two sections, a particularly effective algorithmic solution procedure will be presented.

<sup>1</sup> Another method for achieving this objective is that of adding the functional

$$g(\mu) = \sum_{k=0}^L \left\{ \mu_k^2 - \frac{E}{L+1} \right\}^2$$

to  $f(\mu)$  and then minimizing  $f(\mu) + \lambda g(\mu)$ .

#### 4.3 NONRECURSIVE MODEL

In what is to follow, it will be beneficial to interpret the finite length autocorrelation sequence  $R_{\mu}(n)$  as being the unit-impulse response of a nonrecursive discrete-time system configuration. To verify this postulated interpretation, let us consider the subsystem characterized by the following time-causal nonrecursive operator

$$s(n) = \mu_0 x(n) + \mu_1 x(n-1) + \dots + \mu_L x(n-L) \quad (4.3-1)$$

where  $x(n)$  and  $s(n)$  denote the input and response sequences, respectively, and the  $\mu_k$  are constants which will be subsequently identified with the elements of a real pulse-burst code. The transfer function which corresponds to this operator is then given by

$$H(z) = \mu_0 + \mu_1 z^{-1} + \dots + \mu_L z^{-L} \quad (4.3-2)$$

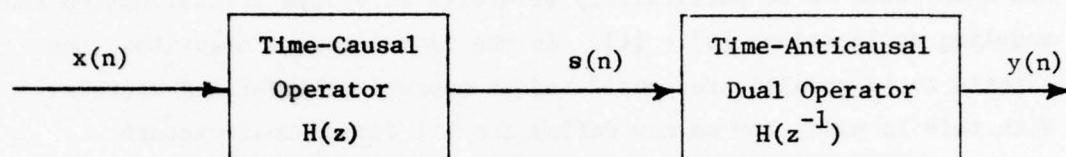
For reasons which will be made clear shortly, let us connect in cascade with operator (4.3-1) its time-anticausal dual. This anticausal dual will be characterized by the nonrecursive operator relationship

$$y(n) = \mu_0 s(n) + \mu_1 s(n+1) + \dots + \mu_L s(n+L) \quad (4.3-3)$$

in which the input sequence  $s(n)$  is equal to the response of time-causal operator (4.3-1). This cascaded configuration is depicted in Figure 4.3-1 where it is noted that the transfer function of time-anticausal operator (4.3-3) is simply  $H(z^{-1})$ . Using standard z-transform theory properties, it follows that the z-transform of this configuration's response to the Kronecker unit-impulse is given by

$$\begin{aligned} Y(z) &= H(z)H(z^{-1}) \\ &= \left[ \sum_{k=0}^L \mu_k z^{-k} \right] \left[ \sum_{n=0}^L \mu_n z^n \right] \end{aligned}$$

A comparison of this expression with relationship (3.5-4), however, indicates that  $Y(z)$  is simply the  $z$ -transform of the autocorrelation sequence  $R_{\mu}(n)$ . In other words, the impulse response of the nonrecursive operator configuration shown in Figure 4.3-1 is equal to the autocorrelation sequence which corresponds to the real pulse-burst code  $\{\mu_0, \mu_1, \dots, \mu_L\}$ .



$$H(z) = \mu_0 + \mu_1 z^{-1} + \mu_2 z^{-2} + \dots + \mu_L z^{-L}$$

FIGURE 4.3-1 CASCADE CONFIGURATION FOR GENERATION OF AUTOCORRELATION SEQUENCE

The generation of a real pulse-burst code which will have a desired autocorrelation behavior has then been equated to that of assigning values to the coefficients of a nonrecursive operator so that its unit-impulse response best matches a desired response (i.e., the ideal autocorrelation sequence (4.2-1)). This equivalency is significant since it is now possible to utilize powerful systems theory modeling algorithms for generating excellent real pulse-burst codes. A particularly effective identification algorithm for this purpose will be presented in the next section.

#### 4.4 LINEARIZATION ALGORITHM

In this section, an algorithmic procedure for selecting the coefficients  $\{\mu_k\}$  which characterize the nonrecursive operator depicted in Figure 4.3-1 so that its unit-impulse response best approximates the ideal



autocorrelation sequence  $R_i(n) = E\delta(n)$  will be presented. The criterion to be minimized is squared error functional (4.2-3) in which the element  $\mu_0$  is held constant at some prespecified value. The ideal code's energy will be normalized at  $E = L+1$  with the objective of encouraging each of these conjectured minimizing code elements to have magnitudes close to one for reasons of efficient signal energy transmission.

The method to be used is the so-called linearization algorithm which has been found to be particularly effective in system identification and modeling applications [3] - [4]. In the linearization algorithm, the signals to be modeled are considered as appropriately defined vectors. With this in mind, let us now define two  $L+1$  dimensional vectors

$$\begin{aligned} y[\mu] &= [y(0), y(1), y(2), \dots, y(L)]' \\ y_i &= [L+1, 0, 0, \dots, 0]' \end{aligned} \tag{4.4-1}$$

where the prime denotes vector transposition. In these representations, the vector  $y[\mu]$  has components  $y(k)$  which correspond to the causal portion of the unit-impulse response of the given nonrecursive operator and therefore the causal portion of the autocorrelation sequence associated with the real pulse-burst code  $\{\mu_k\}$ . We have here suggestively expressed the response vector as an explicit function of the  $L \times 1$  parameter vector

$$\mu = [\mu_1, \mu_2, \dots, \mu_L]' \tag{4.4-2}$$

to emphasize the dependency of  $y[\mu]$  on  $\mu$ . The vector  $y_i$  is seen to be identical to the causal portion of the normalized ideal autocorrelation sequence that is to be approximated. It is only necessary to consider the causal portions of each sequence since the autocorrelation sequences corresponding to real pulse-burst codes are known to be even.

The functional to be minimized (4.2-2) can now be compactly expressed in the standard-inner product format

$$f(u) = (y[u] - y_1) W(y[u] - y_1) \quad (4.4-3)$$

where  $W$  is the  $(L+1) \times (L+1)$  diagonal weighting matrix whose diagonal elements are given by  $w(0), 2w(1), 2w(2), \dots, 2w(L)$ . It is noted that  $y[u] - y_1$  is the error vector which measures the amount by which the actual code's autocorrelation differs from the ideal autocorrelation.

In any descent algorithm, the existing parameter vector is perturbed in a direction so as to cause the functional being minimized to take on a smaller value. With this in mind, let us consider the perturbed functional value

$$f(u+\Delta) = (y[u+\Delta] - y_1) W(y[u+\Delta] - y_1) \quad (4.4-4)$$

where  $\Delta$  is a  $L \times 1$  parameter perturbation vector. The linearization algorithm is based on making the following linearization of the response vector  $y(u+\Delta)$

$$y[u+\Delta] = y[u] + \sum_{k=1}^L \Delta_k \partial y[u] / \partial \mu_k \quad (4.4-5)$$

where the  $\Delta_k$  are the components of the perturbation vector  $\Delta$  and the  $(L+1) \times 1$  vectors  $\partial y[u] / \partial \mu_k$  are the so-called "sensitivity vectors" of the associated nonrecursive operator. These sensitivity vectors yield the differential amount by which the given nonrecursive operator's response changes when a differential variation is made in the component  $\mu_k$ . With reference to Figure 4.3-1, it can be shown that the causal portion of the sensitivity vectors are given by

$$\begin{aligned} (\partial y[u] / \partial \mu_k) &= [\mu_k, \mu_{k-1}, \dots, \mu_0, 0, 0, \dots, 0] \\ &+ [\mu_k, \mu_{k+1}, \dots, \mu_L, 0, 0, \dots, 0] \end{aligned} \quad (4.4-6)$$

for  $k = 1, 2, \dots, L$ . The determination of these sensitivity vectors for a given set of coefficients  $\{\mu_0, \mu_1, \dots, \mu_L\}$  is then straight-

forward and requires only a simple two vector addition operation.

If the linearization of the perturbed response vector as given by expression (4.4-5) is substituted into functional (4.4-4), a quadratic (in  $\Delta$ ) approximation of  $f(\mu+\Delta)$  results. It is readily shown that an optimum selection for the parameter vector perturbation  $\Delta$  to minimize this quadratic approximation must satisfy the following consistent system of  $L$  linear equations in  $L$  unknowns

$$[T_{\mu}' W T_{\mu}] \Delta = T_{\mu}' W \{y_i - y[\mu]\} \quad (4.4-7)$$

where  $T_{\mu}$  is a  $(L+1) \times L$  matrix whose  $k^{\text{th}}$  column vector corresponds to the sensitivity vector  $\partial y[\mu] / \partial \mu_k$  for  $k=1, 2, \dots, L$ .

It has been shown that if the parameter vector  $\mu$  does not render  $f(\mu)$  a relative minimum, then the perturbed vector  $\mu + \alpha \Delta$  will yield a smaller value to the functional being minimized. Here  $\alpha$  is a step size scalar selected in the interval  $0 \leq \alpha \leq 1$  and  $\Delta$  is a solution to relationship (4.4-7). With this in mind, the linearization algorithm as described in Table 4.4-1 is offered. This algorithm has guaranteed convergence and in fact converges in a quadratic manner (e.g., see ref. [3]). A computer program to implement this algorithm is given in section 8.2.

- Step 1      Enter initial guess  $\mu^0$
- Step 2      Calculate  $\partial y[\mu] / \partial \mu_k$   $k = 1, 2, \dots, L$
- Step 3      Evaluate  $T'_\mu$
- Step 4      If  $\| T'_\mu W\{y_i - y[\mu]\} \|^2$  is less than some prescribed small positive values (e.g.,  $10^{-7}$ ), then the algorithm is said to have converged, otherwise go to step 5\*
- Step 5      Solve relationship (4.4-7) for  $\Delta$
- Step 6      Sequentially set  $\alpha = 1, 1/2, 1/4, 1/8, \dots$  and evaluate  $f(\mu + \alpha\Delta)$  until condition  $f(\mu + \alpha\Delta) < f(\mu)$  is first satisfied
- Step 7      Let  $\mu = \mu + \alpha\Delta$  and go to step 2

TABLE 4.4-1      BASIC STEPS OF LINEARIZATION ALGORITHM

#### 4.5 INITIAL CODE SELECTION

The hypothesized functional  $f(\mu)$  which is to be minimized is a quartic function of the code elements  $\mu_k$ . One would therefore anticipate that there will exist a number of different code selections which will render  $f(\mu)$  a relative minimum (i.e., values of the code elements  $\mu_1, \mu_2, \dots, \mu_L$  for which the gradient of  $f(\mu)$  is zero). Some of these "minimizing" codes will have an associated autocorrelation sequence which has a desired impulse-like characteristic while other minimizing codes will not be so characterized. The particular relative minimum code to which the linearization algorithm converges is to a large extent dependent on the initial code selection

$$\{\mu_0^0, \mu_1^0, \dots, \mu_L^0\}$$

\* The quantity  $T'_\mu W\{y_i - y[\mu]\}$  is in fact equal to minus one half the gradient of  $f(\mu)$  (i.e.,  $-0.5 \nabla_\mu f(\mu)$ ) while the notation  $\|x\|^2$  stands for  $x'x$ .



which is made at step 1 of the algorithm as specified in Table 4.4-1. Since the linearization algorithm is of a descent nature, it follows that when the initial code selection has a satisfactory autocorrelation behavior, then the code to which the algorithm converges must be of a superior quality. Thus the initial code selection is the most critical factor in generating suitably good pseudo-optimum codes.

For code lengths in which there exists a Barker code, a natural initial code selection would be the Barker code. On the otherhand, an appropriately chosen real Huffman code would suffice for any code length (e.g., see ref. [1]). Alternatively, a concatenation of shorter length Barker codes has also been found to be effective in constructing reasonably well-behaved initial codes of long length.

In formulating the functional to be minimized, the code element  $\mu_0$  was held fixed so as to prevent the algorithm from converging to an undesired optimum code of length one. It has been empirically determined that different choices of  $\mu_0$  will result in codes which has significantly different energy efficiency factors, normalized maximum side lobe ratios, and, code variances. With this in mind, the linearization algorithm is run with a number of different choices for  $\mu_0$  taken from the set

$$\{\delta, 2\delta, \dots, p\delta\}$$

where typically  $p\delta=1$  with  $\delta$  being a positive number less than one (e.g.,  $\delta=0.1$ ). From the family of  $p$  pseudo-optimum codes which results from each of these fixed  $p$  selections of  $\mu_0$ , it is generally possible to select one which is deemed superior (e.g., one whose energy efficiency is a maximum).

## SECTION 5

### NUMERICAL RESULTS

#### 5.1 PSEUDO-OPTIMUM CODE OF LENGTH 11

The linearization algorithm as described in Section 4.4 was first used to generate a pseudo-optimum code of length 11. It is noted that for this code length, there exists an associated Barker code. With reference to Table 3.4-1, a logical choice for the linearization algorithm's initial code is then given by

$$\mu^0 = [\mu_0^0, 1, 1, -1, -1, -1, 1, -1, -1, 1, -1] \quad (5.1-1)$$

where it is noted that the Barker code's initial element value 1 has been replaced by the fixed parameter  $\mu_0^0$ . The linearization algorithm was then used to generate the pseudo-optimum codes which corresponded to each of the following ten selections for  $\mu_0^0$ .

$$\mu_0^0 = \{0.1, 0.2, 0.3, \dots, 1\}$$

In this algorithmic procedure, the error weights  $w(n)$  were all set to one. The normalized maximum side lobe ratio, the energy efficiency factor, and, the code variance (as defined in Section 3.3) which corresponds to each of the pseudo-optimum codes iteratively generated for these  $\mu_0^0$  selections are shown in Table 5.1-1. The best code from this family is deemed to be the one associated with  $\mu_0^0 = 0.5$  since maximum energy efficiency utilization was of primary concern.<sup>1</sup> A plot of this pseudo-optimum code and its associated autocorrelation function is shown in Figure 5.1-1.

<sup>1</sup>If maximum side lobe reduction were of primary concern, then the code corresponding to  $\mu_0^0 = 0.1$  would have been chosen.

$\mu_0$	$\rho$	$\epsilon$	$\lambda$
0.1	0.211	0.589	0.000909
0.2	0.289	0.456	0.115
0.3	0.367	0.376	0.00782
0.4	0.431	0.322	0.0136
0.5	0.473	0.285	0.021
0.6	0.440	0.259	0.0298
0.7	0.410	0.241	0.0398
0.8	0.390	0.230	0.0510
0.9	0.378	0.224	0.0633
1.0	0.372	0.223	0.0763

TABLE 5.1-1 INITIAL CODE SELECTION-LENGTH 11

In terms of normalized maximum side lobe ratio, the pseudo-optimum code shown in Figure 5.1-1 is superior by 6.36db over the Barker code of length 11, and, by 6.00db over the complex Huffman code of length 11 as shown in Figure 3.5-2. Although this is but one example of a short length real pulse-burst code, it does illustrate how one may generate effective real codes using an algorithmic approach.

To further compare the inherent signal characteristics of the pseudo-optimum, Barker, and Huffman codes of length 11, their associated ambiguity functions were calculated by means of relationship (3.1-5) and are shown in Figure 5.1-2. In these plots, the ambiguity surface is sliced along the  $\omega=0$  axis so that the associated autocorrelation function corresponds to the leading edge of the surface as is readily apparent in the cases of the Barker and Huffman codes. A careful examination of these ambiguity surfaces reveals that the pseudo-optimum and Barker codes are clearly superior to the Huffman code. More over, the pseudo-optimum is somewhat better behaved than the Barker, particularly relative to autocorrelation behavior.

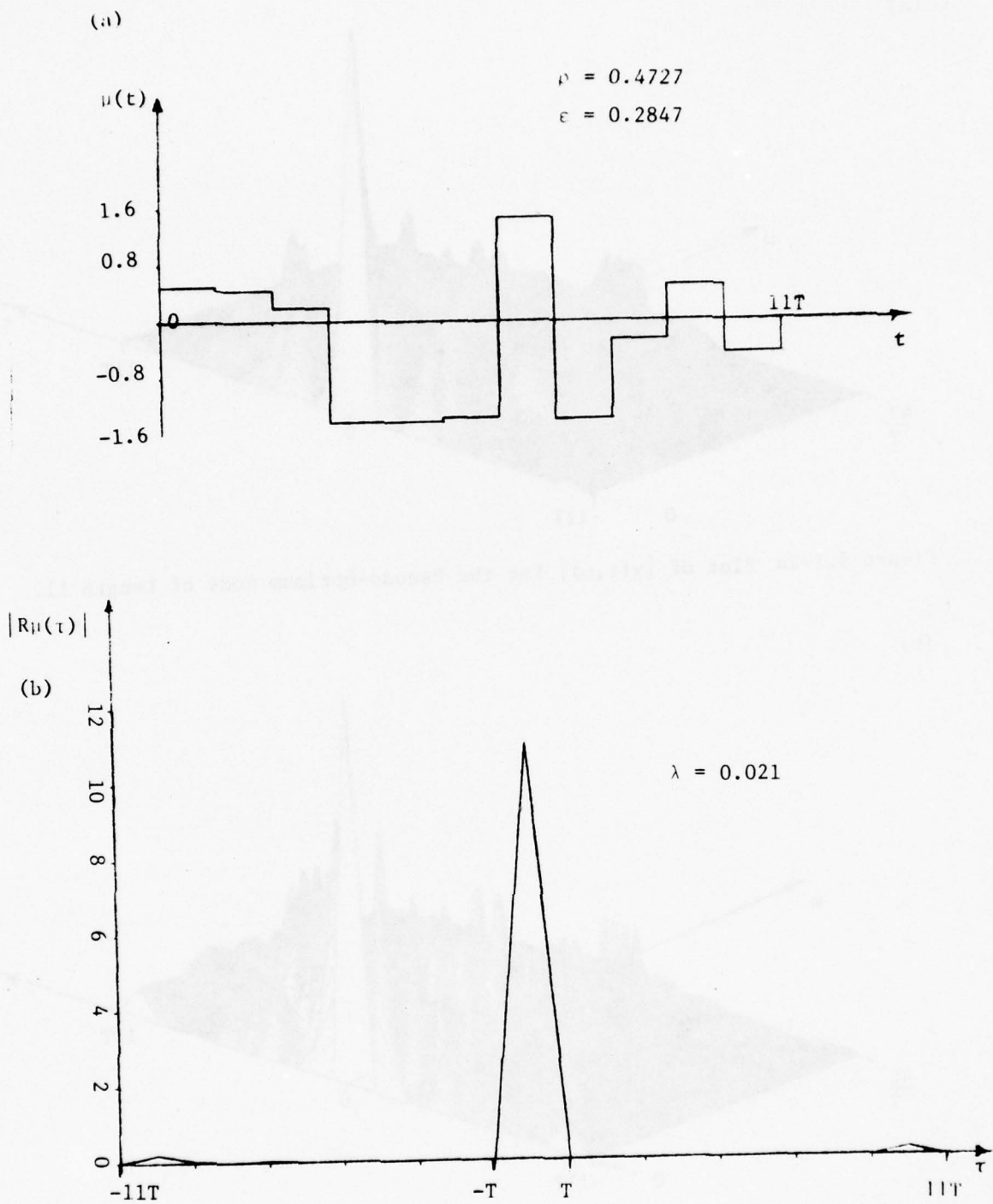


FIGURE 5.1-1 PSEUDO-OPTIMUM (a) plot of code,  
 (b) associated autocorrelation function



(a)

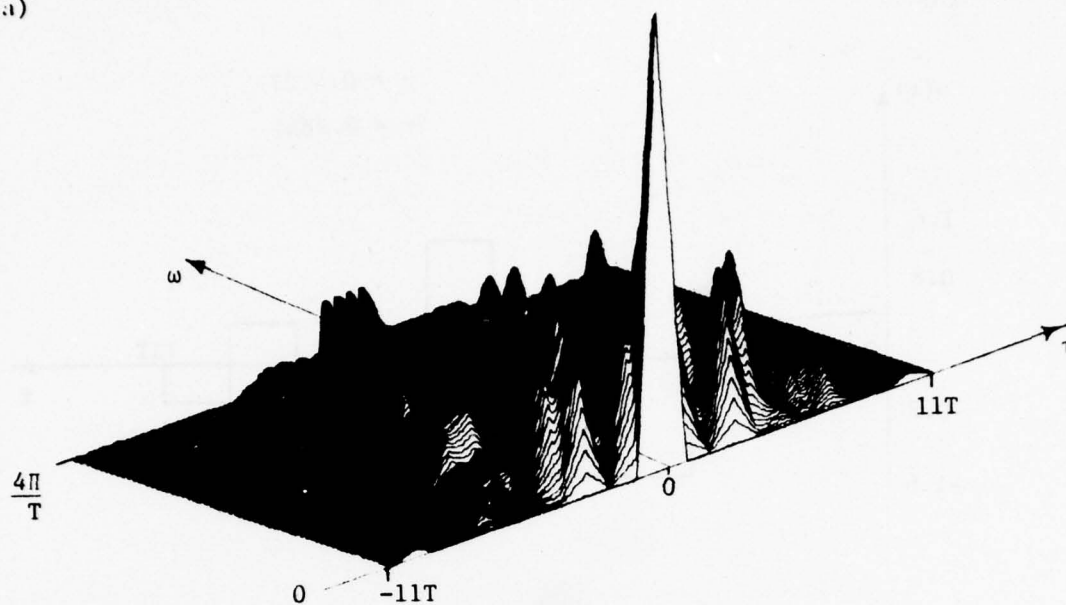


Figure 5.1-2a Plot of  $|\chi(\tau, \omega)|$  for the Pseudo-Optimum Code of Length 11.

(b)

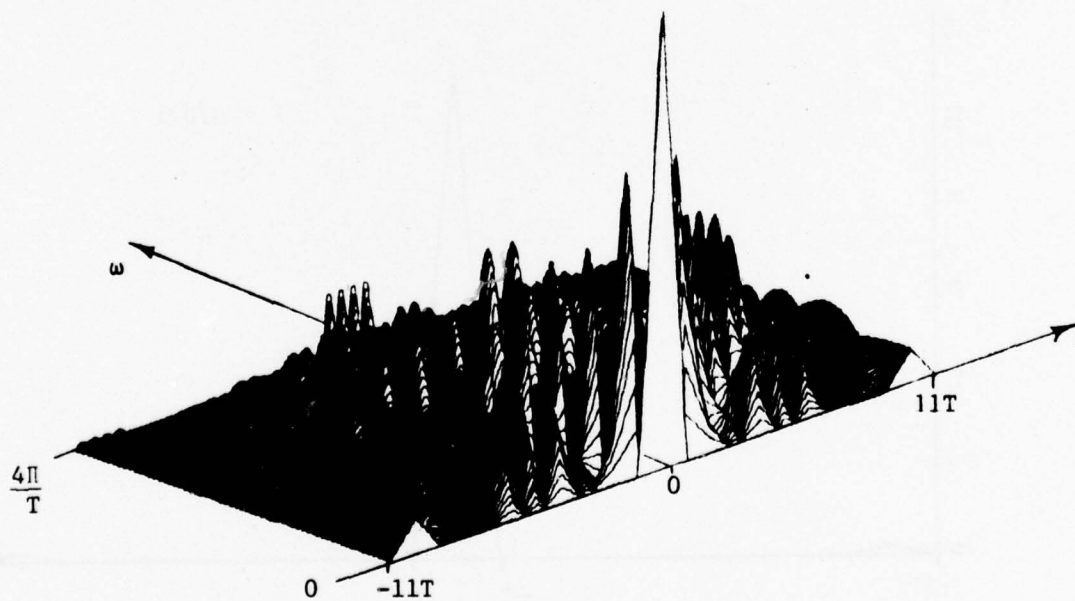


Figure 5.1-2b Plot of  $|\chi(\tau, \omega)|$  for the Huffman Code of Length 11.

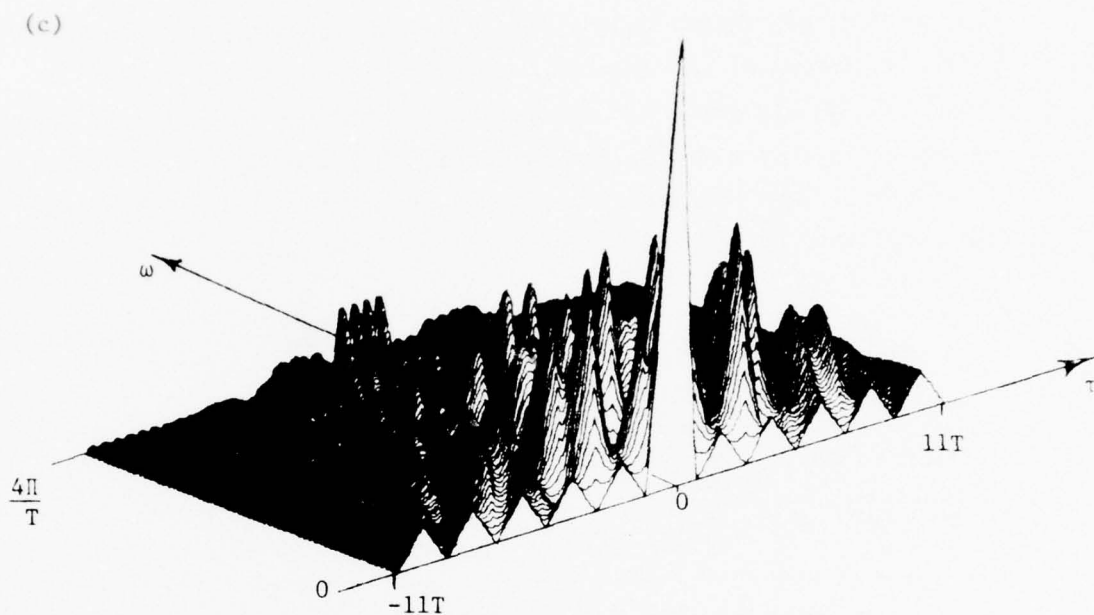


Figure 5.1-2c Plot of  $|\chi(\tau, \omega)|$  for the Barker Code of Length 11.

## 5.2 PSEUDO-OPTIMUM CODE OF LENGTH 128

The true effectiveness of the proposed algorithm for synthesizing real pulse-burst codes is made evident when constructing long length codes. To demonstrate this assertion, a real pulse-burst code of length 128 was next generated. When considering this relatively long length code, the choice of the initial code  $\mu_0^0, \mu_1^0, \dots, \mu_{127}^0$  used in step 1 of the algorithm becomes even more critical as well as difficult to make. In this example, the real code of length 128 as tabulated in reference [1] was used to initiate the algorithm. This initial code has excellent characteristics as shown in Table 5.2-1.

	Normalized Maximum Side Lobe $\lambda$	Energy Efficiency $\rho$	Code Variance $\epsilon$
Initial Code	$9.508 \times 10^{-4}$	0.3348	0.2757
Pseudo-Optimum Code	$8.125 \times 10^{-8}$	0.3426	0.2862

TABLE 5.2-1 RELEVANT CHARACTERISTICS OF REAL PULSE-BURST CODES OF LENGTH 128

Using this initial code, the algorithm was found to converge to a pseudo-optimum code whose normalized maximum side lobe ratio was found to have decreased by a factor of  $10^{-4}$  over that of the initial code. The relevant parameters which characterize this pseudo-optimum code are also shown in Table 5.2-1. In addition, a plot of the codes magnitude and its associated autocorrelation and ambiguity functions are given in Figure 5.2-1. It must be mentioned that these excellent characteristics and ambiguity function behavior can only be approximated in practice due to the inherent incapability of exactly reproducing the precise amplitudes for the code length required.

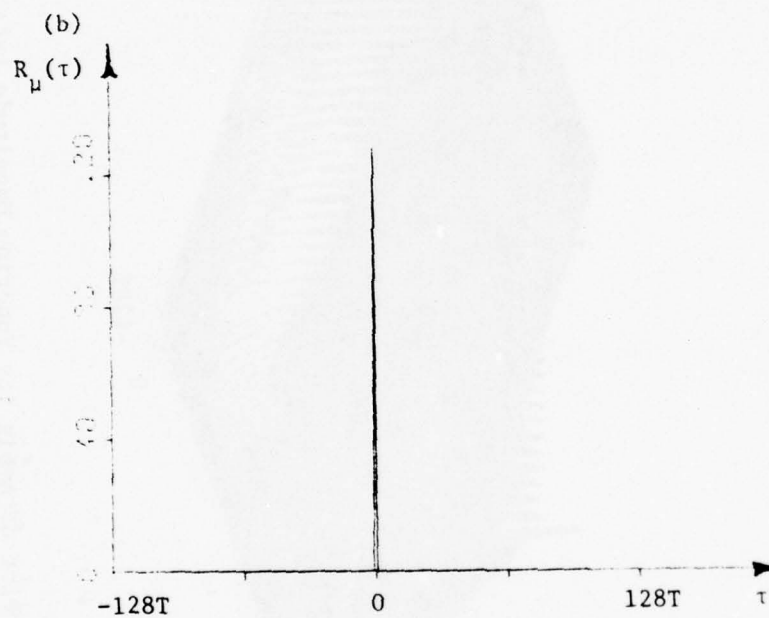
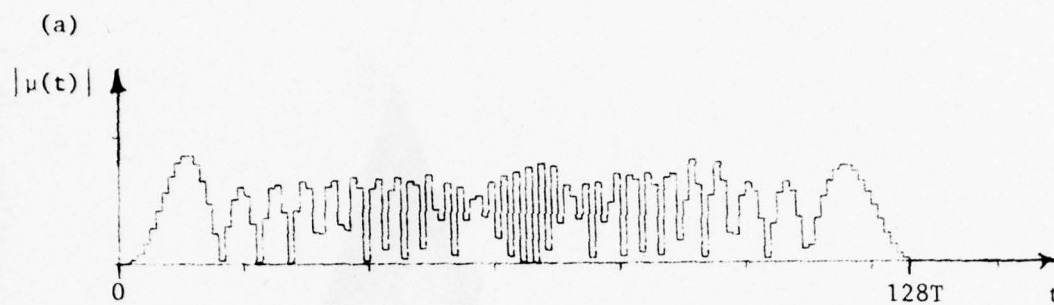


Figure 5.2-1 Pseudo-Optimum Code of Length 128

(a) Magnitude of Code  $|\mu(t)|$ , (b) Corresponding Autocorrelation Function  $R_\mu(\tau)$



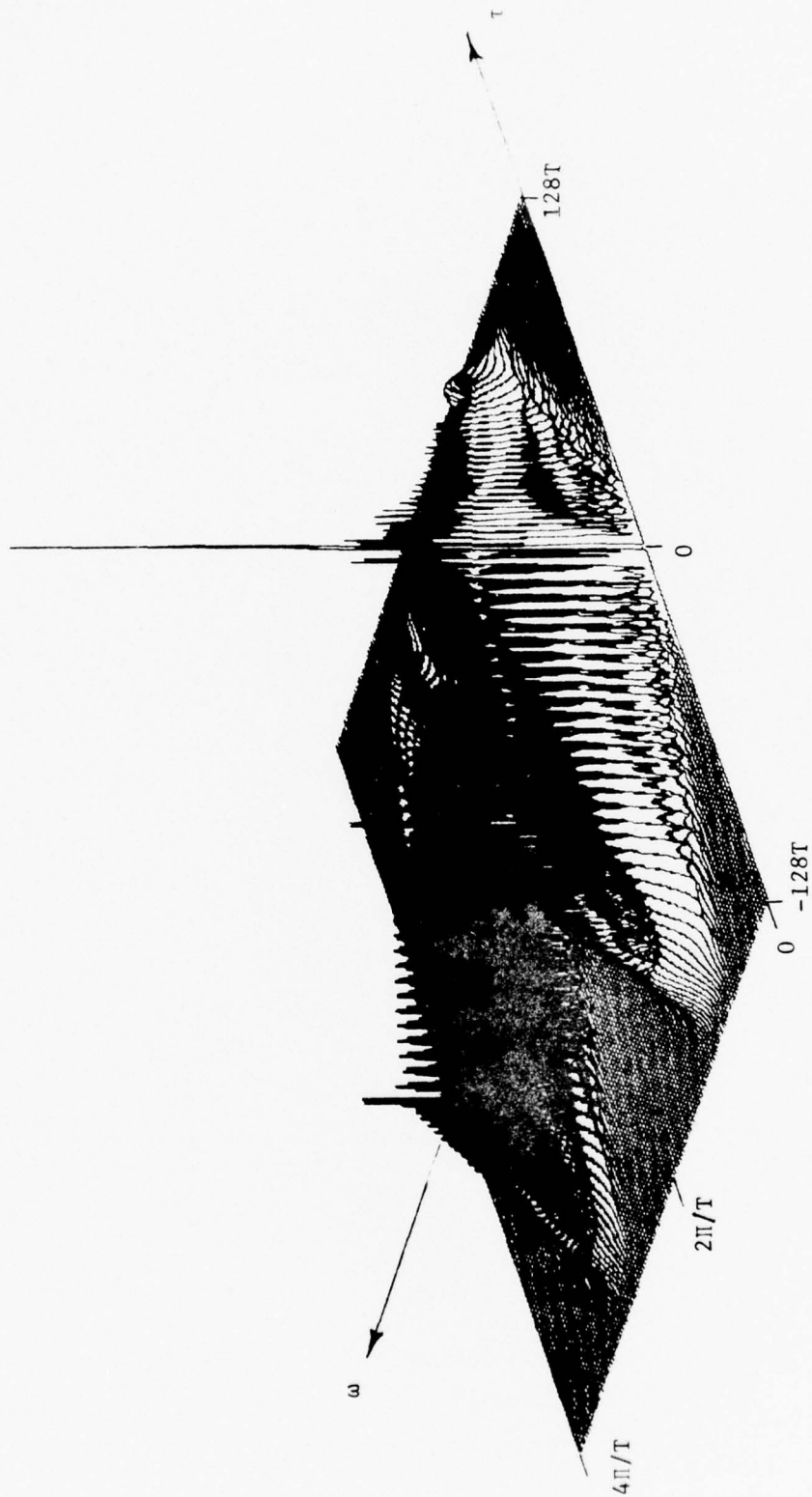


Figure 5.2-1 Plot of Ambiguity Function Magnitude  $|\chi(\tau, \omega)|$  for Pseudo-Optimum Code of Length 128

## SECTION 6

### CONCLUSIONS AND RECOMMENDATIONS

The iterative procedure as herein described for synthesizing real pulse-burst codes has proven to be effective in all examples treated. Namely, the pseudo-optimum code to which the algorithm converges has been found to possess such desirable characteristics as having an associated impulse-like autocorrelation function and a well-behaved ambiguity function. Furthermore, the algorithm's convergence rate is quadratic in nature thereby offering a computationally efficient code synthesis procedure. This procedure therefore promises to be a very useful tool for constructing good real pulse-burst signals.

To achieve the algorithm's true potential, however, it is essential that a systematic method for constructing a suitable initial code be developed. The method suggested by Akroyd [1] appears to satisfy this requirement although further investigations along this line need be made. For example, it might be possible to further adapt some of the techniques as given by Schroeder [7] to construct appropriate initial codes. The importance of this initial code selection cannot be over emphasized.

Another consideration which must be made is that of generating codes whose energy efficiency is appropriately large. Initial investigations of how one might achieve this capability, while still maintaining the algorithm's basic features, have been made. In essence, this requires that an inner product which gives a positive measure of energy efficiency be added to the functional  $f(\mu)$ . A minimization of this new functional would then tend to simultaneously generate a real pulse-burst code which has a relatively large energy efficiency utilization as well as an impulse-like autocorrelation behavior.

## SECTION 7

### REFERENCES

- [1] Ackroyd, M. H., Synthesis of Efficient Huffman Sequences, IEEE Trans. on Aerospace and Electronic Systems, Vol. AES-8, No. 1, January 1972, pp 2-8.
- [2] Bird, G. J. A., RADAR PRECISION AND RESOLUTION, John Wiley & Sons, Inc., New York, 1974.
- [3] Cadzow, J. A., System Modeling, an Efficient Algorithmic Approach, Presented at the 1975 Conf. Information Sciences and Systems, The Johns Hopkins University, Baltimore, MD., April 1975.
- [4] Cadzow, J. A., Recursive Digital Filter Synthesis Via Gradient Based Algorithms, IEEE Trans. on Acoustics, Speech, and Signal Processing, Vol. ASSP-24, No. 5, October, 1976, pp 349-355.
- [5] Caprio, J. R., Strictly Complex Impulse-Equivalent Codes and Subsets With Very Uniform Amplitude Distributions, IEEE Trans. on Information Theory, Vol. IT-15, No. 6, November, 1969, pp 695-706.
- [6] Cook, E. C. and M. Bernfeld, RADAR SIGNALS, Academic Press, New York, 1967.
- [7] Schroeder, M. R., Synthesis of Low-Peak-Factor signals and Binary Sequences with Low Autocorrelation, IEEE Trans. on Information Theory, Vol. IT-16, pp 85-89, January 1970.

# SECTION 8

## 8.1 APPENDIX A

### AMBIGUITY FUNCTION PLOT PROGRAM

```
PROGRAM MAIN(INPUT,OUTPUT,TAPE5=INPUT
$           ,TAPE6=OUTPUT
$ ,TAPE1,TAPE2,TAPE3,TAPE4,TAPE7,TAPE8,TAPE9)
```

```
C      *** THIS PROGRAM GENERATES THE AMBIGUITY *
C      *** FUNCTION AND PLOTS IN THREE      *
C      *** DIMENSIONAL SPACE.                *
```

```
COMPLEX D,B1COM,B2COM,DTEMP,XTEMP,EX1,EX2,CSUM
$           ,A,TEMP
DIMENSION D(128),B1COM(128),B2COM(128),X(2561)
$           ,MASK(4001),DATA(256)
$           ,DIN(128),TEMP( 43),A(43,128)
```

```
REWIND 1
REWIND 2
REWIND 3
REWIND 4
REWIND 7
REWIND 8
REWIND 9
PI=3.1415926535898
```

```
C      *** T ---- SAMPLING TIME                *
C      *** L ---- NUMBER OF CODE LENGTH        *
C      *** NF --- NUMBER OF LINES FOR EVERY    *
C      ***                2*PI/T WHICH ARE PLOTTED *
C      ***                PARALLEL TO THE TIME AXIS *
C      *** DIN -- REAL PART OF EACH CODE        *
C      ***                ELEMENT                *
C      *** D ---- CODE ARRAY                    *
```

T=1.

```
L=128
AL=L
L1=L/3+1
L2=L1*2
LH=L/2
L2M=(L-1)*2-1
```

```
NF=64
NF2=NF*2
```



```

NF3=NF+3
NFC=NF+6
NFM1=NF-1

```

```

      READ(2,*) (DIN(M),M=1,L)
      DO 14 M=1,L
      MM=M*2-1
14  D(M)=CMPLX(DIN(M),0.0)
      CSUM=CMPLX(0.0,0.0)
      DO 30 M=1,L
30  CSUM=CSUM+CONJG(D(M))*D(M)
      SUM=REAL(CSUM)
      SCA=SQRT(AL/SUM)
      DO 41 M=1,L
41  D(M)=SCA*D(M)
      *WRITE(6,100)
100  FORMAT(/,3X,* CODE D *)
      PRINT *,(D(M),M=1,L)
      CNE=0.

```

```

C      *** SUMMATION INVOLVED IN AMBIGUITY      *
C      *** FUNCTION IS COMPUTED BY FFT.          *

```

```

      DO 7 K=1,2
      DO 1 IP=1,L
      CALL SECOND(TIME)
      PRINT*,"TIME IS ",TIME
      II=IP-1
      NNF=2*(IP+ONE)
      IF(NNF.EQ.0) GO TO 21
      DO 2 M=1,NNF
2  DATA(M)=CMPLX(0.0,0.0)
21  IS=IP+ONE
      IF(IS.GT.L) GO TO 22
      DO 3 M=IS,L
      MT=M*2-1+2
      DTEMP=D(M)*CONJG(D(M-II-ONE))
3  DATA(MT)=REAL(DTEMP)
      DATA(MT+1)=AIMAG(DTEMP)
      CONTINUE
22  LL=2*(L+1)+1
      DO 18 M=LL,NF2
      DATA(M)=0.0
18  CONTINUE
      IF(L.LE.NF) GO TO 25

```

```

C      *** COMPUTES BY NOT USING FFT.          *

```

```

27  CALL AF0UR(DATA,NF,L,ONE,T)
      GO TO 26
29  CALL FOUR1(DATA,NF,-1)
26  IF(IP.GT.L1) GO TO 31
      DO 6 M=1,NF
      MT=M*2-1
6  A(IP,M)=CMPLX(DATA(MT),DATA(MT+1))
      IF(IP.NE.L1) GO TO 1
      DO 32 MJ=1,NF

```

```

      DO 33 MI=1,L1
33  TEMP(MI)=A(MI,MJ)
      IF(K.EQ.2) GO TO 35
      WRITE(1,*) TEMP
      GO TO 32
35  WRITE(4,*) TEMP
32  CONTINUE
      GO TO 1
31  IF(IP.GT.L2) GO TO 43
      IIP=IP-L1
      DO 9 M=1,NF
      MT=M*2-1
      9  A(IIP,M)=CMPLX(DATA(MT),DATA(MT+1))
      IF(IIP.NE.L1) GO TO 1
      DO 34 MJ=1,NF
      DO 35 MI=1,L1
35  TEMP(MI)=A(MI,MJ)
      IF(K.EQ.2) GO TO 37
      WRITE(3,*) TEMP
      GO TO 34
37  WRITE(7,*) TEMP
34  CONTINUE
      GO TO 1
43  IIP=IP-L2
      DO 44 M=1,NF
      MT=M*2-1
      44  A(IIP,M)=CMPLX(DATA(MT),DATA(MT+1))
      IF(IP.NE.L) GO TO 1
      DO 45 MJ=1,NF
      DO 46 MI=1,L1
46  TEMP(MI)=A(MI,MJ)
      IF(K.EQ.2) GO TO 49
      WRITE(8,*) TEMP
      GO TO 45
49  WRITE(9,*) TEMP
42  CONTINUE
      1  CONTINUE
      ONE=1.
      7  CONTINUE

```

```

C      *** THIS PROGRAM HAS THE CAPABILITY OF      *
C      *** PLOTTING FOR THE INTERVAL  $-6\pi/T$  TO *
C      ***  $+6\pi/T$  ALONG OMEGA AXIS.             *

```

```

CALL PLOTS
ISTEP=10
ISTEP1=ISTEP+1
DEL=T/ISTEP
IPOINT=L*ISTEP
L2M=(IPOINT*2+1)/10
IP21=IPOINT*2+1
IBASE=NF3
NF3P=NF3+1
NF6P=NF6+1
NFD=NF*5+1
ILINE=0
CALL PLOT3D(10,0.0,X,0.0,0.0023,0.03125

```

```

$      , -0.036, ILINE, IP21
$ , -45.0, -20.0, 10.0, .25, 20.0, MASK, 0)
REWIND 1
REWIND 3
REWIND 4
REWIND 7
REWIND 8
REWIND 9

```

```

C      *** EVERY LINE IS DRAWN PARALLEL TO THE *
C      *** TIME AXIS. THE LINES WHICH SHOULD BE *
C      *** HIDDEN BY PREVIOUS LINES ARE MASKED. *

```

```

DO 13 I=NF3P,NFD
  ILINE=I-NF3
  IR=NF6P+1-I
  II=NF3+1-I
  II=-II
  OMG=PI*II*2./(NF*T)
  EX1=CMPLX(0.0,OMG*T/2.)
  EX2=CMPLX(0.0,OMG*T)
  IF(IR.LE.NF3) GO TO 16
  IND=IR-IBASE
  IF(IND.NE.1) GO TO 12
  IF(I.EQ.NF3P) GO TO 12
  IBASE=IBASE-NF
  GO TO 12
16 IND=I-IBASE
  IF(IND.NE.NF) GO TO 12
  IBASE=IBASE+NF
12 IF(IND.NE.1) GO TO 50
  REWIND 1
  REWIND 3
  REWIND 4
  REWIND 7
  REWIND 8
  REWIND 9
50 READ(1,*) TEMP
  DO 38 M=1,L1
33 B1COM(M)=TEMP(M)
  READ(3,*) TEMP
  DO 39 M=1,L1
  MT=L1+M
39 B1COM(MT)=TEMP(M)
  READ(8,*) TEMP
  DO 47 M=1,L1
  MT=L2+M
47 B1COM(MT)=TEMP(M)
  READ(4,*) TEMP
  DO 42 M=1,L1
42 B2COM(M)=TEMP(M)
  READ(7,*) TEMP
  DO 40 M=1,L1
  MT=L1+M
40 B2COM(MT)=TEMP(M)
  READ(9,*) TEMP
  DO 48 M=1,L1

```

```

      MT=L2+M
43  B2CDM(MT)=TEMP(M)
      XTEMP=T*CEXP(EX1)*SINC(OMG*T/2.)*B1CDM(1)
      X(IPJINT+1)=CABS(XTEMP)
      DO 10 J=1,L
      JJ=J-1
      DO 10 K=1,ISTEP
      KK=K
      EX1=CMPLX(0.0,OMG*(T-DEL*KK)/2.)
      EX2=CMPLX(0.0,OMG*(2.*T-DEL*KK)/2.)
      XTEMP=(T-DEL*KK)*CEXP(EX1)
      $ *SINC(OMG*(T-DEL*KK)/2.)*B1CDM(J)
      $ + DEL*KK*CEXP(EX2)
      $ *SINC(OMG*DEL*KK/2.)*B2CDM(J)
      XX=CABS(XTEMP)
      KT=JJ*ISTEP+K
      X(IPJINT+1-KT)=XX
      X(IPJINT+1+KT)=XX
10  CONTINUE
      CALL PLOT3D(10,0.0,X,0.0,0.0023,0.03125
      $ , -0.036,ILINE,IP21
      $ , -45.0, -20.0, 10.0, .25, 20.0, MASK, C)
      IF(I.NE.NF3P) GO TO 13
24  WRITE(6,140)
140  FORMAT(/,3X,*OMEGA = J*)
      DO 23 IM=1,L2M
      BASE=10*(IM-1)
      IBS=BASE+1
      IBL=BASE+10
      PRINT *,(X(M),M=IBS,IBL)
23  CONTINUE
13  CONTINUE
      CALL EFPLDT
      STOP
      END

```



SUBROUTINE AF0UR(DATA,NF,L,ONE,T)

C

\*\*\* COMPUTES FOURIER TRANSFORM

\*

```
DIMENSION DATA(256),DT(256)
COMPLEX EX,SUM,TMP
PI=3.1415926535898
DO 1 IP=1,NF
  IPP=IP*2-1
  IIP=IP-1
  SUM=CMPLX(0.0,0.0)
  LP=L+1
  DO 2 N=2,LP
    II=2*N-1
    NN=N-1
    X=-2.*PI*IIP*NN*T/NF
    TMP=CMPLX(0.0,X)
    EX=CEXP(TMP)
    TMP=CMPLX(DATA(II),DATA(II+1))
    SUM=TMP*EX+SUM
  2 CONTINUE
  DT(IPP)=REAL(SUM)
  DT(IPP+1)=AIMAG(SUM)
1 CONTINUE
NF2=NF*2
DO 3 I=1,NF2
  3 DATA(I)=DT(I)
RETURN
END
```

## 8.2 APPENDIX B

### PSEUDO-OPTIMUM CODE ALGORITHM PROGRAM

```

PROGRAM MAIN(INPUT,OUTPUT,TAPE5=INPUT
$              ,TAPE6=OUTPUT
$              ,TAPE1,TAPE2,TAPE3)

C      *** THIS PROGRAM COMPUTES THE OPTIMUM *
C      *** PULSE BURST CODE. *

COMMON R(255),N,NN,AN,Q(255),DJ,NP
DIMENSION D(127),DD(127),P(127),DT(127)
$ ,S(127),QQ(255),DIN(127)
REAL LAM

C      *** D ---- CODE ARRAY *
C      *** R ---- CORRELATION ERROR ARRAY *
C      *** N ---- THE LARGEST INDEX OF CODE *
C      *** THE LENGTH OF CODE IS N+1 *
C      *** Q ---- WEIGHTING FACTOR OF MEAN *
C      *** SQUAR ERROR *
C      *** LAM -- ADJUSTABLE FACTOR TO GET *
C      *** BETTER EFFICIENCY *
C      *** (WEIGHTING OF PENALTY *
C      *** FUNCTIONAL) *
C      *** BET -- ADJUSTABLE FACTOR TO GET *
C      *** BETTER SPIKE TO SIDERJBE *
C      *** RATIO *

N=127
NP=N+1
NP2=N+2
NH=N/2
NHM=NH-1
AN=N
NN=2*N+1
LAM=0.0
BET=50.

WRITE(6,350) LAM
350 FORMAT(/,3X,*LAMBDA = *,F10.5)
WRITE(6,360) BET
360 FORMAT(/,3X,*BETA = *,F10.5)
340 FORMAT(/,3X,*Q MATRIX : *)
READ*,(Q(M),M=1,21)

```

```

      READ*, (Q(M),M=22,41)
      DO 32 M=42,NN
32  Q(M)=1.
      DO 35 M=1,NN
35  CQ(M)=Q(M)
      READ *,DO,(D(M),M=1,N)
      SUM=DO*DO
      DO 60 M=1,N
60  SUM=SUM+D(M)*D(M)
      FAC=(AN+1.)/SUM
      FAC=SQRT(FAC)
      DO=DO*FAC
      DO 61 M=1,N
61  D(M)=D(M)*FAC
      PERD=CORRE(D,S,LAM)
      CALL PVEC(P,GRAD,D,LAM,S)
      I=0
      CALL CONVT(R,N)
      WRITE(6,100) I,PERD,GRAD
      WRITE(6,200)
      CALL WR(P,N)
      WRITE(6,300)
      PRINT *,DO
      CALL WR(D,N)
      WRITE(6,310)
      CALL WR(R,NN)
      CALL EFVA(DO,D,R(N+1),N)
      CALL CONVT(R,N)
      DO 20 M=1,N
20  DD(M)=D(M)
      I=1
      M1=1

```

C            \*\*\* COMPUTES P VECTOR            \*

```

11  CALL PVEC(P,GRAD,D,LAM,S)
      PERD=CORRE(D,S,LAM)
      DO 66 M=1,N
66  SUM=SUM+P(M)*P(M)
      ALF=(AN+1.)/SUM
      ALF=SQRT(ALF)
      IF(ALF.GT.2.) ALF=2.0

```

C            \*\*\* SEARCHING THE STEP SIZE            \*

```

68  DO 13 J=1,10
      PRINT *,ALF
      DO 14 K=1,N
14  D(K)=DD(K)+ALF*P(K)
      ERO=CORRE(D,S,LAM)
      IF(ERO.LE.PERD) GO TO 15
      ALF=ALF/2.
13  CONTINUE
15  PERD=ERO
      DO 18 M=1,N
18  DD(M)=D(M)
      SUM=C.

```

```

ALL=(1./2.)*9
IF(ALF.LE.ALL) GO TO 17
IF(GRAD.LT..0001) GO TO 17
IF(J.EQ.10) GO TO 17
IF(I.EQ.50) GO TO 17
I=I+1
GO TO 11

```

C            \*\*\* ADJUSTS WEIGHTING Q            \*

```

17 SUM=0.
   DO 33 M=1,NN
33 SUM=SUM+R(M)*R(M)
   DO 34 M=1,NN
34 Q(M)=QQ(M)+BET*R(M)*R(M)/SUM
   WRITE(6,100) I,PERD,GRAD
100 FORMAT(/,10X,*ITER. = *,I3,5X,
$ *ERROR = *,E11.3,
$5X,*GRADIENT = *,F20.5)
   WRITE(6,200)
200 FORMAT(1X,* P VECTOR :*)
   CALL WR(P,N)
   WRITE(6,300)
300 FORMAT(/,1X,* CODE D :*)
   PRINT *,DO
   CALL WR(D,N)
   CALL CONV(T,R,N)
   WRITE(6,310)
310 FORMAT(/,1X,* CORRELATION R :*)
   CALL WR(R,NN)
   CALL EFVA(DO,D,R(N+1),N)
   WRITE(6,340)
   CALL WR(Q,NN)

```

C            \*\*\* COMPUTES CORRELATION FOR TRUNCATED            \*  
C            \*\*\* CODE            \*

```

   CALL TRUNC(DO,D,N)
   PTR=CORRE(D,S,LAM)
   CALL CONV(T,R,N)
   WRITE(6,310)
   CALL WR(R,NN)
   CALL CONV(T,R,N)
   IF(M1.EQ.4) GO TO 38
   IF(M1.EQ.1) GO TO 38
   M1=M1+1
   GO TO 11
38 STOP
END

```



SUBROUTINE PVEC(P,GRAD,D,LAM,S)

```

C      *** COMPUTES FRECHET MATRIX      *
C      *** AND FINDS P VECTOR.          *
      *
      COMMON R(255),N,NN,AN,Q(255),DO,NP
      DIMENSION FRM(127,127),P(127),S(127),B(127)
      $ ,D(127)
      REAL LAM
      DO 1 J=1,N
      US=N+1-J
      UL=US+N
      DS=J+1
      DL=DS+N
      DO 2 I=1,NN
      IF(I.GT.UL) GO TO 3
      III=I-US
      IF(III)      3,4,5
3     UK=0.
      GO TO 6
4     UK=DO
      GO TO 6
5     II=I-US
      UK=D(II)
6     IF(I.LT.DS) GO TO 9
      III=I-DL
      IF(III) 7,8,9
7     II=DL-I
      DK=D(II)
      GO TO 10
8     DK=DO
      GO TO 10
9     DK=0.
10    IF(I-NP) 38,39,2
38    FRM(I,J)=UK+DK
      GO TO 2
39    S(J)=UK+DK
2     CONTINUE
1     CONTINUE
      REWIND 1
      DO 23 I=1,N
      DO 24 J=1,N
      SUM=0.
      DO 25 K=1,N
25    SUM=1.*FRM(K,I)*FRM(K,J)*Q(K)+SUM
      P(J)=SUM+Q(N+1)*S(I)*S(J)
24    CONTINUE
      WRITE (1) P
23    CONTINUE
      DO 26 I=1,N
      SUM=0.
      DO 27 K=1,N
27    SUM=FRM(K,I)*R(K)*Q(K)*1.+SUM
      B(I)=SUM+Q(N+1)*R(N+1)*S(I)
26    CONTINUE
      REWIND 1
      DO 36 I=1,N

```

```

      READ (1) P
      DO 37 J=1,N
37  FRM(I,J)=P(J)
36  CONTINUE
      DO 31 I=1,N
31  FRM(I,I)=LAM+FRM(I,I)
      SUM=0.
      DO 32 I=1,N
32  SUM=SUM+D(I)*D(I)
      SUM=SQRT(SUM/AN)
      DO 33 I=1,N
33  S(I)=SIGN(SUM,D(I))

```

C                    \*\*\* COMPUTES GRADIENT                    \*

```

      DO 34 I=1,N
34  B(I)=B(I)-LAM*(D(I)-S(I))
      SUM=0.
      DO 13 I=1,N
13  SUM=SUM+B(I)*B(I)
      SUM=SUM*4.
      GRAD=SQRT(SUM)/AN
      CALL SIMQ(FRM,B,N, ING)
      IF( ING.EQ.0) GO TO 35
      WRITE(5,101)
101  FORMAT(/,3X,*MATRIX IS SINGULAR*)
35  DO 17 I=1,N
17  P(I)=B(I)
      RETURN
      END

```

FUNCTION CORRE(D,S,LAM)

```

C      *** COMPUTES THE CORRELATION OF CODE      *
C      *** AND MEAN SQUAR ERROR.                *

COMMON R(255),N,NN,AN,Q(255),DO,NP
DIMENSION D(127),S(127)
REAL LAM
N1=N-1
DO 1 I=1,N1
  II=N+1+I
  R(II)=D(I)*DO
  JJ=N+1-I-1
  DO 2 J=1,JJ
2  R(II)=R(II)+D(J)*D(J+I)
1  CONTINUE
  R(N+1)=DO*DO
  DO 3 I=1,N
3  R(N+1)=R(N+1)+D(I)*D(I)
  R(NN)=D(N)*DO
  DO 4 I=1,N
  II=NN+1-I
4  R(I)=R(II)
  DO 5 I=1,N
  II=N+1+I
  R(I)=-R(I)
5  R(II)=-R(II)
  R(N+1)=AN-R(N+1)+1.
  ERO=0.
  DO 6 I=1,NN
6  ERO=Q(I)*R(I)*R(I)+ERO
  SUM=0.
  DO 7 I=1,N
7  SUM=SUM+(D(I)-S(I))*(D(I)-S(I))
  ERO=ERO+LAM*SUM
  CORRE=ERO
  RETURN
END

```

SUBROUTINE EFVA(DO,D,RX,N)

```

C      *** COMPUTES EFFICIENCY AND CODE      *
C      *** VARIANCE.                          *
      DIMENSION D(1)
      AN=N
      DM=DO*DO
      DO 25 M=1,N
      DQ=D(M)*D(M)
25    DM=AMAX1(DM,DQ)
      EF=RX/((AN+1.)*DM)
      WRITE(6,320) EF
320  FORMAT(/,1CX,*EFFICIENCY = *,F10.7)
      EF=EF*DM
      EF=SQRT(EF)
      SUM=(DO-EF)**2
      DO 26 M=1,N
      ABD=ABS(D(M))
26    SUM=(ABD-EF)**2+SUM
      VAR=SUM/RX
      WRITE(6,330) VAR
330  FORMAT(/,1UX,*CODE VARIANCE = *,F10.7)
      RETURN
      END

```

SUBROUTINE TRUNC(X1,X,N)

```

C      *** TRUNCATES THE CODE.                *
      DIMENSION X(1)
      X1=X1*100.
      IX1=X1
      X1=IX1/100.
      DO 1 I=1,N
      X(I)=X(I)*100.
      IX=X(I)
1    X(I)=IX/100.
      RETURN
      END

```



SUBROUTINE CONV1(R,N)

C           \*\*\* CONVERT TO CORRELATION FROM           \*  
C           \*\*\* CORRELATION ERROR OR VICE VERSA.       \*

DIMENSION R(1)  
AN=N  
DO 23 M=1,N  
II=2\*N+2-M  
R(M)=-R(M)  
23 R(II)=R(M)  
R(N+1)=AN-R(N+1)+1.  
RETURN  
END

SUBROUTINE WR(XX,NNN)

C           \*\*\* THIS SUBROUTINE IS USED TO PRINT       \*  
C           \*\*\* OUT THE RESULTS FOR CONVENIENCE.       \*

DIMENSION XX(1)  
NLAS=NNN/10  
DO 51 I=1,NLAS  
IS=10\*(I-1)+1  
IL=IS+9  
WRITE(6,370) (XX(J),J=IS,IL)  
370 FORMAT(/,3X,10(E11.2))  
51 CONTINUE  
IIS=NLAS\*10  
IF(IIS.EQ.NNN) GO TO 1  
IS=NLAS\*10+1  
WRITE(6,370) (XX(J),J=IS,NNN)  
1 RETURN  
END

# MISSION of *Rome Air Development Center*

RADC plans and conducts research, exploratory and advanced development programs in command, control, and communications (C<sup>3</sup>) activities, and in the C<sup>3</sup> areas of information sciences and intelligence. The principal technical mission areas are communications, electromagnetic guidance and control, surveillance of ground and aerospace objects, intelligence data collection and handling, information system technology, ionospheric propagation, solid state sciences, microwave physics and electronic reliability, maintainability and compatibility.

